Microscale C-O-S isotope signatures record microbial sulfate reduction in ancient deep subsurface pyrite-calcite-barite assemblages

Eric Runge[1,2*], Vanessa Fichtner[1,3], Mikael Tillberg[1], Martin Whitehouse[4], Henrik Drake[1]

[1]Department of Biology and Environmental Science, Linnaeus University, Kalmar, Sweden
[2]GeoZentrum Nordbayern, Friedrich-Alexander Universität (FAU) Erlangen-Nürnberg, Erlangen, Germany
[3]Department of Geobiology, University of Göttingen, Göttingen, Germany
[4]Laboratory for Isotope Geology, Swedish Museum of Natural History, Stockholm, Sweden

Correspondence to: Eric Runge (eric.runge@fau.de)

Abstract. The deep biosphere harbors diverse microbial communities amounting to a substantial fraction of Earth's biomass for much of its history. Analyses of fracture-hosted minerals (e.g., pyrite, calcite) and their C-O-S isotope signatures are beginning to establish a fossil record of subsurface microbial communities and their relationship with major geological events. Fracture-coating pyrite from deep within the Fennoscandian Shield records the largest ^{34}S-enrichment observed on Earth to date ($\delta^{34}S$ = +147 ‰) – likely the result of late-stage Rayleigh distillation during closed-system microbial sulfate reduction (MSR). This implies even heavier S isotope values for the complementary sulfate reservoir during pyrite formation, possibly recorded in coeval sulfate minerals such as barite [$BaSO_4$]. However, barite has been poorly explored as an archive of ancient deep subsurface biosignatures, particularly in samples with extreme ^{34}S-enrichment in pyrite. Here, we compiled published microscale $\delta^{13}C_{calcite}$, $\delta^{18}O_{calcite}$, and $\delta^{34}S_{pyrite}$ data with new secondary ion mass spectrometry (SIMS) $\delta^{18}O_{barite}$ and $\delta^{34}S_{barite}$ analyses from two localities on the Fennoscandian Shield (Forsmark and Laxemar, Southeastern Sweden), aiming to constrain the record of microbial processes in barite. We identified two groups of barites distinguished by their distinct $\delta^{18}O/\delta^{34}S$ trends. Comparison of these trends with $\delta^{13}C$ values of cogenetic calcite reveals variable associations with sulfate-dependent anaerobic oxidation of methane (AOM) and organotrophic sulfate reduction (OSR). Strongly ^{13}C-depleted calcite ($\delta^{13}C_{calcite} < -40$ ‰), indicating a relationship with AOM, almost exclusively occurs in the steeper trending Group 1. Evidence for barite affected by OSR ($\delta^{13}C_{calcite} > -30$ ‰) occurs in both groups and dominates the shallower trending Group 2. The different trends likely resulted from an interplay of MSR pathways (AOM vs. OSR) and variations in sulfate reduction rates (SRR), which we attribute to the relative abundances of sulfate and electron donors in the parent fluid of barite. Lower sulfate and electron donor abundances likely permitted methanogenesis and AOM at lower SRR, resulting in a steeper $\delta^{18}O/\delta^{34}S$ trend in Group 1 barite. Conversely, higher sulfate and electron donor abundances inhibited methanogenesis and AOM, favoring OSR at a higher SRR, which is reflected by the shallower $\delta^{18}O/\delta^{34}S$ trend in Group 2 barite. Comparison between the $\delta^{34}S_{pyrite}$ range (−53.9 to +131.7 ‰) and the $\delta^{34}S_{barite}$ range (+7.6 to +52.0 ‰) across both localities demonstrates that the sulfate reservoir corresponding to extremely ^{34}S-enriched pyrite is not recorded in barite. The discrepancy between barite and pyrite could reflect their formation in separate microenvironments or barite undersaturation at high degrees of Rayleigh distillation. Our study highlights the need for coupled microscale C-O-S analyses in fracture-hosted mineral assemblages to understand metabolic processes in the ancient deep biosphere, while stressing that these records are affected by local hydrogeochemical conditions.

hat gelöscht: Multiple microscale stable
hat gelöscht: metabolic processes
hat gelöscht: barite-
hat gelöscht: sulfur
hat gelöscht: .
hat gelöscht: $\delta^{34}S_{pyrite}$
hat gelöscht: $\delta^{13}C_{calcite}$
hat gelöscht: and $\delta^{18}O_{barite}$
hat gelöscht: / Äspö
hat gelöscht: how barite records
hat gelöscht: history
hat verschoben (Einfügung) [1]
hat gelöscht: .
hat gelöscht: across both localities
hat gelöscht: with
hat gelöscht: We identified two groups of barite distinguished by their distinct $\delta^{18}O/\delta^{34}S$ trends, which is proposed to record different MSR-related processes based on cogenetic $\delta^{13}C_{calcite}$ data. Although there is overlap between the metabolic processes recorded in both groups, the steeper trending Group 1 was dominantly associated with sulfate-dependent anaerobic oxidation of methane (AOM), whereas the shallower trending Group 2 was dominated by organoclastic sulfate reduction (OSR).
hat nach oben verschoben [1]: The different trends likely resulted from an interplay of MSR pathways (AOM vs.
hat gelöscht: OSR), as well as variations in sulfate reduction rates (SRR) and fractionation-related isotope enrichment ($^{34}\varepsilon$), attributed to paleoenvironmental ratios of sulfate to electron donor abundances. Lower sulfate/ electron donor ratios favored methanogenesis and AOM at lower SRR, whereas higher ratios inhibited methanogenesis and favored OSR at higher SRR. A preservation bias against extremely ^{34}S-enriched barite due to undersaturation at high degrees of Rayleigh distillation likely explains its absence in the deep subsurface. Our study highlights the need for microscale multiple stable isotope signatures
hat gelöscht: strongly

1 Introduction

The average depth of the 122 °C isotherm in the continental crust is 4.8 km, defining a vast rock volume that is cooler than the upper known temperature limit of life (Takai et al., 2008). For this reason, fractures and rock pores in the continental crust represent one of the largest habitable environments on Earth (Magnabosco et al., 2018). This 'deep biosphere' hosts diverse communities of chemolithoautotrophic primary producers and heterotrophic microorganisms, including methanogens, methanotrophs, and sulfate reducers (Chivian et al., 2008; Kieft et al., 2018; Ruff et al., 2024; Stevens and McKinley, 1995; Wu et al., 2016). Recent estimates of the total biomass of the deep biosphere vary (Bar-On et al., 2018; Magnabosco et al., 2018; McMahon and Parnell, 2014), but its significant impact on global biogeochemical cycles is generally accepted. Before the rise of land plants, the deep subsurface may have even held the majority of Earth's total biomass (McMahon and Parnell, 2018). Indeed, portions of the continental crust have been continuously habitable since 1.1 billion years ago (Ga) and may have experienced habitable periods since 1.9 Ga (Drake and Reiners, 2021). Understanding the diversity and biogeochemical impact of the deep biosphere throughout Earth's history requires robust and geologically stable biosignatures. However, the deep biosphere fossil record remains patchy and poorly understood (Gustafsson and Drake, 2025; Ivarsson et al., 2020).

Minerals and their stable isotope ratios can represent valuable biosignatures in deep time (Runge et al., 2023). For instance, the largest magnitudes of S isotope fractionation between sulfate and sulfide ($^{34}\varepsilon = \delta^{34}S_{sulfate} - \delta^{34}S_{sulfide}$) are associated with kinetic isotope effects (KIE) during microbial sulfate reduction (MSR). Depending on the microbial strain and environmental parameters, such as the temperature, or the availability of sulfate and electron donors (organic matter or H_2), $^{34}\varepsilon$ induced by MSR can vary between 0 and ~70 ‰ (Bradley et al., 2016; Chambers et al., 1975; Farquhar et al., 2003; Habicht et al., 2002; Ries et al., 2009; Sim et al., 2011; Wing and Halevy, 2014; Wortmann et al., 2001). These signatures can be recorded in ^{34}S-depleted authigenic sulfide minerals (e.g., pyrite) (Halevy et al., 2023; Pasquier et al., 2025; Strauss, 1997). Microbial sulfate reduction can also be coupled with anaerobic oxidation of methane (AOM), which is well supported in the deep subsurface (Bell et al., 2022; Drake et al., 2015, 2017; Kotelnikova, 2002). Microbially produced methane is ^{13}C-depleted relative to CO_2 by up to 95 ‰ (Whiticar, 1999), hence methane oxidation via AOM can result in the precipitation of strongly ^{13}C-depleted calcite (Aloisi et al., 2002; Campbell et al., 2002; Feng et al., 2010; Lin et al., 2011; Natalicchio et al., 2012; Reitner et al., 2005). On the other hand, calcite precipitation resulting from organotrophic sulfate reduction (OSR) typically reflects the less ^{13}C-depleted organic carbon substrate. Notably, dating of fracture-coating minerals (adularia Rb/Sr, calcite U/Pb, and hematite U-Th/He) co-genetic to biosignatures in pyrite and calcite record ancient MSR deep within the Fennoscandian Shield between the Ordovician (460 ± 30 Ma) and the Neogene (13.7 ± 0.6 Ma) (Drake et al., 2017, 2018, 2021). Thus, the combination of S and C isotope ratios is a powerful approach for reconstructing ancient MSR pathways.

During the early stages of MSR, $\delta^{18}O_{sulfate}$ increases via a minor KIE and an equilibrium isotope effect (EIE) between H_2O and intermediate S species (e.g., sulfite) before their re-oxidation to sulfate (Antler et al., 2013; Böttcher et al., 1999; Brunner et al., 2005; Fritz et al., 1989; Mizutani and Rafter, 1973; Wortmann et al., 2007) (Fig. 1). The slopes of $\delta^{18}O/\delta^{34}S$ trends are strongly controlled by the sulfate reduction rate (SRR). At a lower SRR, the equilibration of intermediate S species with water

hat gelöscht: Fractures

hat gelöscht: . The average depth of the 122 °C isotherm, the upper known temperature limit of life , in the continental crust is 4.8 km, implying a vast habitable rock volume

hat gelöscht: It has been suggested that

hat gelöscht: before the rise of land plants

hat gelöscht: for up to

hat gelöscht: time windows

hat gelöscht: billion years ago (Ga)

hat gelöscht: sulfur

hat gelöscht: $\delta^{34}S_{SO4}$–$\delta^{34}S_{H2S}$

hat gelöscht:) or temperature,

hat gelöscht: Thermochemical sulfate reduction (TSR) becomes dominant at temperatures exceeding 100 °C and can involve sulfur isotope fractionation via a kinetic isotope effect (KIE) at up to $\Delta^{34}S_{SO4-H2S} \approx 20$ ‰ at 100 °C; . Equilibrium fractionation at 100 °C could reach $\Delta^{34}S_{SO4-H2S} \approx 43$ ‰ , representing a theoretical maximum for TSR.¶

hat gelöscht: sulfate-dependent

hat gelöscht: Methane

hat gelöscht: typically

hat gelöscht: because microbial methanogenesis induces strong carbon isotope fractionation ($^{13}\varepsilon = \delta^{13}C_{CO2}$–$\delta^{13}C_{CH4} \approx$

hat gelöscht: ‰; . This

hat gelöscht: lead to ^{13}C-enrichment in the residual inorgar ... [1]

hat gelöscht: authigenic carbonates (e.g.,

hat gelöscht:) as a result of methane oxidation

hat gelöscht: During organoclastic

hat gelöscht: ; i.e., MSR coupled to

hat gelöscht: oxidation of

hat gelöscht: substrates)

hat gelöscht: AOM, the $\delta^{18}O$ of residual sulfate

hat gelöscht: kinetic

hat gelöscht: and equilibration

hat gelöscht: sulfur

hat gelöscht: and $\delta^{18}O_{H2O}$

hat gelöscht: . Thus, the combination of sulfur, carbon, and ... [2]

hat gelöscht: $\delta^{18}O_{SO4}$/ $\delta^{34}S_{SO4}$

hat gelöscht: during the early stages of MSR is primarily ... [3]

hat gelöscht: intracellularly re-oxidized to sulfate (Fig. 1) ... [4]

hat gelöscht: cell-specific

hat gelöscht: a higher fraction of sulfur intermediates is ox ... [5]

hat gelöscht: $\delta^{18}O_{H2O}$

is more pronounced and $\delta^{18}O_{sulfate}$ rises more rapidly relative to $\delta^{34}S_{sulfate}$ (i.e., a steeper slope). At a higher SRR, the rise $\delta^{18}O_{sulfate}$ relative to $\delta^{34}S_{sulfate}$ is less pronounced (i.e., a shallower slope). In addition, AOM and OSR can result in different slopes at similar SRR (Antler et al., 2014), and the slopes resulting from AOM differ between methane diffusion-limited settings (e.g., marine sediments: steeper trend) and methane-in-excess environments (e.g., cold seeps, stratified estuaries: shallower trend) (Antler et al., 2015) (Fig. 1). Owing to the preferential consumption of $^{32}SO_4^{2-}$ by microorganisms, MSR in a closed system (i.e., when the SRR exceeds the resupply of sulfate) can produce ^{34}S-enriched sulfate in the residual porewater (Anderson et al., 1987; Jørgensen et al., 2004; Rudnicki et al., 2001; Zaback et al., 1993). This process has resulted in $\delta^{34}S_{pyrite}$ values of up to +147 ‰ in deep fractures of the Fennoscandian Shield, the most extreme ^{34}S-enrichment yet reported (Drake et al., 2018). This implies an even more ^{34}S-enriched complementary sulfate reservoir during pyrite formation. Barite [$BaSO_4$] is a robust archive of $\delta^{18}O_{sulfate}$ and $\delta^{34}S_{sulfate}$ values in its parent fluid because its precipitation is associated with minimal stable isotope fractionation and it is thermodynamically table and poorly soluble (Crockford et al., 2019; Griffith and Paytan, 2012; Han et al., 2025; Paytan et al., 1998, 2002; Turchyn and Schrag, 2004, 2006; Wood et al., 2021). Thus, the co-variation of $\delta^{18}O_{barite}$ and $\delta^{34}S_{barite}$ values may record past and extant environmental conditions and microbial S cycling, complementing the C-O-S isotope records in pyrite and calcite. However, pyrite-calcite-barite assemblages are poorly explored archives of ancient deep subsurface microbial processes, particularly in samples containing extremely ^{34}S-enriched pyrite.

Here, we compile previously published microscale $\delta^{13}C_{calcite}$, $\delta^{18}O_{calcite}$, and $\delta^{34}S_{pyrite}$ data from multiple deep drill cores taken at two localities on the Fennoscandian Shield (Forsmark and Laxemar/Äspö, Southeastern Sweden) with new secondary ion mass spectrometry (SIMS) $\delta^{18}O_{barite}$ and $\delta^{34}S_{barite}$ analyses from the same drill cores. In most cases, barite occurred in fractures that contained associated pyrite and/or calcite. Although we did not detect extreme ^{34}S-enrichment in barite, our results demonstrate barite records an ancient archive of OSR and AOM, while highlighting that these archives are affected by local hydrogeochemical conditions.

hat gelöscht: a stronger increase in $\delta^{18}O_{SO4}$

hat gelöscht: $\delta^{34}S_{SO4}$

hat gelöscht: trend

hat gelöscht: a lower fraction of sulfur intermediates is oxidized, leading to stronger increase of $\delta^{34}S_{SO4}$ relative to $\delta^{18}O_{SO4}$

hat gelöscht: trend). Sulfate reduction rates in the deep subsurface are generally low , but relative variations in SRR may result from differences in temperature, abundance of sulfate-reducing microorganisms, competition with other microorganisms, availability of electron donors, quality of organic substrates, and sulfate concentrations ….

hat gelöscht: produce

hat gelöscht: trends

hat gelöscht: . The trends produced by

hat gelöscht: gas

hat gelöscht: total sulfate reduction rates exceed

hat gelöscht: In extreme cases, this

hat gelöscht: produced

hat gelöscht: fracture systems

hat gelöscht: largest

hat gelöscht: , which may be recorded by coeval and geologically stable sulfate minerals

hat gelöscht: Barite [$BaSO_4$] is a robust archive of $\delta^{34}S_{SO4}$ and $\delta^{18}O_{SO4}$ values in its parent fluid because i) its precipitation is associated with minimal stable isotope fractionation and ii) it can resist diagenetic and metamorphic overprints over geological time . Notably, ^{34}S-enriched barite is a commonly used proxy for the paleostratigraphic position of the sulfate-methane transition zone (SMTZ) in sedimentary environments, where barite forms under sulfate-limited conditions affected by AOM . Stable isotope analysis of recently precipitated minerals on drill core equipment from the Äspö Hard Rock Laboratory (Sweden) indicated that combining pyrite and barite records is a promising approach for interpreti ... [6]

hat gelöscht: new secondary ion mass spectrometry (SIMS ... [7]

hat gelöscht: ba

hat gelöscht:

hat gelöscht: previously published $\delta^{13}C_{calcite}$, $\delta^{18}O_{calcite}$, and ... [8]

hat gelöscht: could be correlated with

hat gelöscht: from the same fracture.

hat gelöscht: find extremely

hat gelöscht: enriched

hat gelöscht: in

hat gelöscht: samples, the

hat gelöscht: . These biosignature records

hat gelöscht: strongly controlled

hat gelöscht: paleoenvironmental conditions. We suggest t ... [9]

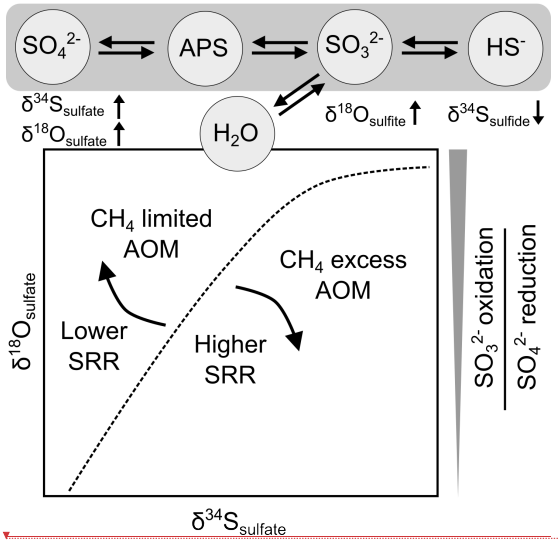


Figure 1: Controls on δ¹⁸O/δ³⁴S trends during the early stages of microbial sulfate reduction (MSR). The intracellular reduction of sulfate to sulfide (HS^-), proceeds via multiple reversible steps, including the activation of adenosine 5'phosposulfate (APS) and reduction to sulfite (SO_3^{2-}). The kinetic isotope effect (KIE) associated with MSR produces ^{34}S-depleted sulfide and ^{34}S-enriched residual sulfate. Concerning O, the KIE associated with MSR is small, and the equilibrium isotope exchange (EIE) between sulfate and water is kinetically inhibited. However, intermediate S species such as sulfite readily exchange O isotopes with water and become relatively ^{18}O-enriched. Intracellular re-oxidation of this sulfite produces ^{18}O-enriched sulfate. The δ¹⁸O/δ³⁴S trends in residual sulfate are controlled by the expression of the EIE associated with sulfite-water exchange relative to the sulfate reduction rate (SRR). This expression becomes more pronounced when the SRR is lower, or when anaerobic oxidation of methane (AOM) occurs under methane (CH_4) limited conditions, resulting in a steeper slope. After Wortmann et al. (2007), Antler et al. (2013, 2014, 2015), Han et al. (2025).

2 Methods

2.1 Materials and sampling

The sampled barite-bearing fractures are from Proterozoic crystalline bedrock at Forsmark, Laxemar, and Äspö (Southeastern Sweden) (see Drake et al. (2018) for details on the geological setting). Laxemar and Äspö are situated at the Baltic Sea coastline, and only ca. three kilometers apart, hence we consider them as one site (i.e., Laxemar) in this study. Drill cores were mainly obtained by triple-tube drilling conducted by the Swedish Nuclear Fuel and Waste Management Co. This drilling technique preserves fragile minerals on fracture surfaces, facilitating the investigation of ancient biological activity in deep fracture systems. Barite was sampled from fractures in a total of 40 drill cores. The samples represented depths ranging from 60 to 1,660 m below sea level. The exact locations of the boreholes are provided in the Supplementary Data Table. Sample

characterization and mineral identification were performed directly on the fracture surfaces using a FEI QUANTA FEG 650 Scanning Electron Microscope (SEM) equipped with an integrated energy dispersive spectroscopy (EDS, Oxford T-Max 80 detector) under low-vacuum conditions. The acceleration voltage was 20 kV, and the instrument was calibrated with a cobalt standard. The barite grains were then hand-picked from the fracture surface under a microscope, included in several epoxy mounts (2.5 cm diameter), and polished to expose the cross-sections of the grains. The polished grains were examined using SEM prior to SIMS analysis to detect growth zonation and avoid impurities and cracks.

2.2 Secondary-ion mass spectrometry (SIMS) analysis of barite ($\delta^{18}O$ and $\delta^{34}S$)

Secondary-ion mass spectrometry (SIMS) was conducted on a CAMECA IMS1280 ion probe at the NordSIMS lab, Swedish Museum of Natural History, Stockholm. The analytical routines for S and O isotope analyses of barite follow those described by Drake et al. (2024), which are based on the approaches by Whitehouse (2013) for S and Heinonen et al. (2015) for O. The samples were sputtered using a $^{133}Cs^+$ primary beam with 20 kV incident energy and a beam current of ~3 nA, which was rastered over a 5 × 5 µm area during analysis. Each analysis comprised 40 s pre-sputter to remove the gold coating over a 15 × 15 µm area, centering of the secondary beam in the field aperture, and data acquisition in 12 four-second integration cycles. Secondary ion signals (^{32}S and ^{34}S or ^{16}O and ^{18}O) were detected simultaneously using two Faraday detectors with a common mass resolution of 4,860 (M/ΔM) for S and 2,430 (M/ΔM) for O. Data were normalized for instrumental mass fractionation using the S0327 reference material, with a conventionally determined $\delta^{34}S$ value of +22.0±0.3 ‰ and $\delta^{18}O$ value of +11.0±0.1 ‰ (Liseroudi et al., 2021). All results are reported as $\delta^{34}S_{V\text{-}CDT}$ (Ding et al., 2001) for S and $\delta^{18}O_{V\text{-}SMOW}$ (Coplen, 1995) for O. The typical uncertainties after propagating the within-run and external uncertainties from the standard measurements were ±0.2 ‰ (1σ) for $\delta^{34}S$ and between ±0.2 and ±0.6 ‰ (1σ) for $\delta^{18}O$ values. The previously published calcite $\delta^{18}O_{V\text{-}PDB}$ values were recalculated to $\delta^{18}O_{V\text{-}SMOW}$ for comparability with barite using the formula $\delta^{18}O_{V\text{-}SMOW} = 1.03092 \times \delta^{18}O_{V\text{-}PDB} + 30.92$. All SIMS data, including previously published data, are compiled in the Supplementary Data Table.

2.3 Statistical analysis

Statistical analysis of 366 paired $\delta^{18}O_{barite}/\delta^{34}S_{barite}$ data was performed using a Gaussian Mixture Model (GMM), which is a useful tool for classifying multivariate stable isotope data (Göhring et al., 2016). GMM was done via the Python module Scikit-learn (Pedregosa et al., 2011). Data from Forsmark and Laxemar were merged to achieve a larger barite samples size, and a sensitivity test was conducted to exclude an influence of merging localities on GMM performance (see Supplementary Figure S2). Nevertheless, the resulting clusters should not be regarded as globally representative and may differ for barite from other areas. Since the clustering result of GMM is sensitive to outliers, we first performed an outlier test via density-based spatial clustering of applications with noise (DBSCAN) to identify points that do not belong to a dense region in our bivariate data frame. The minimum points to form a dense region was set to four and the neighborhood radius (ε = 0.5) was estimated based on a k-distance plot (Supplementary Fig. S1A). In total, 22 data points were indicated as outliers and excluded prior to GMM

hat gelöscht: sulfur (n = 354)
hat gelöscht: oxygen (n = 221)
hat gelöscht: sulfur
hat gelöscht: oxygen
hat gelöscht: sulfur
hat gelöscht: oxygen
hat gelöscht: sulfur
hat gelöscht: oxygen
hat gelöscht: Dataset
hat gelöscht: Cluster

(Supplementary Fig. S1B). To select the appropriate number of clusters in our barite $\delta^{18}O/\delta^{34}S$ dataset, we identified the best-fit model by calculating the Bayesian Information Criterion (BIC) as a function of number of clusters. The resulting BIC values show a clear minimum for two clusters (Fig. S2A). Random state optimization for GMM was performed over a range of zero to four, yielding zero at the minimum BIC. York regression was used to calculate the slopes and r^2 values of the resulting clusters (Supplementary Fig. S2B) (York et al., 2004). Notably, our dataset contains data points from two localities (i.e., Laxemar and Forsmark), whereas Laxemar provides the dominant fraction (323 vs. 21 for S). Deriving clusters that robustly distinguish OSR- and AOM-affected barite requires consistent behavior of these clusters across localities. Hence, we tested the sensitivity of our GMM approach to differences between localities by excluding Forsmark and repeating the same procedure described for the entire dataset. After excluding the Forsmark data, the BIC-guided decision for a two-cluster model remains robust (Supplementary Fig. S2C). Additionally, the resulting slopes of the individual clusters changed minimally after excluding Forsmark data (Supplementary Figs. S2B, S2D). Thus, we used the cluster assignment and slopes resulting from GMM of the whole dataset to interpret our dataset. In concert, these observations strongly support a two-cluster GMM approach for classifying our barite $\delta^{18}O/\delta^{34}S$ dataset.

hat gelöscht: Cluster analysis of the barite $\delta^{18}O$ and $\delta^{34}S$ data was performed using a Gaussian Mixture Model (GMM) via the Python module Scikit-learn . The optimal number of components for the GMM was calculated to be three using the Bayesian Information Criterion (BIC). However, the three components yielded regression lines with negative slopes for the resulting clusters, which is inconsistent with naturally occurring fractionation trends in the $\delta^{18}O$–$\delta^{34}S$ space. Thus, we chose to perform GMM with two components, consistent with the qualitative assumption that sulfate reduction in our system is dominated by two end-member processes (i.e., organoclastic sulfate reduction and anaerobic oxidation of methane). Random state optimization was performed over a range of zero to ten, yielding zero at the minimum BIC. Main axis regression was used to calculate the slopes and R^2 values for the resulting clusters.¶

3 Results and discussion

3.1 Pyrite-calcite barite assemblages record ancient microbial sulfate reduction in the deep subsurface

hat gelöscht: We investigated samples from

Coupled $\delta^{34}S_{pyrite}$ and $\delta^{13}C_{calcite}$ signatures provide evidence of ancient organotrophic sulfate reduction (OSR) and sulfate-dependent anaerobic oxidation of methane (AOM) in deep subsurface fractures at Forsmark and Laxemar (Drake et al., 2013, 2015, 2018, 2021). The compiled data from Forsmark and Laxemar showed a $\delta^{34}S_{pyrite}$ range of −53.9 to +131.7 ‰, a $\delta^{18}O_{calcite}$ range of +10.5 to +28.1 ‰, and a $\delta^{13}C_{calcite}$ range of −93.1 to +36.5 ‰ (Drake et al., 2017, 2018) (Table 1, Figs. 2-3). A prominent role of thermochemical sulfate reduction (TSR) in these localities has been ruled out because of the large apparent $^{34}\varepsilon$ between plausible $\delta^{34}S_{sulfate}$ values of fracture fluids in these systems and pyrite (55 to 66 ‰; Drake et al., 2021). Moreover, TSR generally occurs at temperatures >100 °C (Machel, 2001), which is inconsistent with fluid inclusion homogenization temperatures and clumped isotope thermometry indicating formation temperatures <100 °C of coeval calcite (Drake et al., 2018; Herlambang et al., 2023). Thus, the wide $\delta^{34}S_{pyrite}$ range (−53.9 to +131.7 ‰) was interpreted to reflect Rayleigh distillation during microbial sulfate reduction (MSR) in semi-closed fracture systems, producing ^{34}S-depleted sulfide and extremely ^{34}S-enriched sulfate (Drake et al., 2018). The overall ranges of $\delta^{18}O_{barite}$ (−0.9 to +19.7 ‰) and $\delta^{34}S_{barite}$ (+7.6 to +52.0 ‰) across both localities are consistent with MSR, which can produce ^{18}O- and ^{34}S-enrichment in the residual sulfate pool (Antler et al., 2013, 2014, 2015; Brunner et al., 2005; Drake et al., 2018; Han et al., 2025; Jørgensen et al., 2004; Rudnicki et al., 2001; Wortmann et al., 2007; Zaback et al., 1993). These observations strongly suggest a record of MSR in co-genetic barite from Forsmark and Laxemar.

hat gelöscht: exhibiting

hat gelöscht: ‰

hat gelöscht: 2-3). This range

hat gelöscht: .

The extremely high $\delta^{34}S_{pyrite}$ values at Forsmark and Laxemar imply the presence of an even more ^{34}S-enriched sulfate reservoir potentially archived in co-genetic barite. To detect this archive and investigate its relationship with OSR and AOM, we

hat gelöscht: the record of these microbial processes in ancient barite [$BaSO_4$],

analyzed $\delta^{34}S_{barite}$ and $\delta^{18}O_{barite}$ in the same drill cores that were previously sampled for $\delta^{34}S_{pyrite}$ and $\delta^{18}O_{calcite}$, and $\delta^{13}C_{calcite}$ analysis (Drake et al., 2017, 2018) (Figs. 2,3; Table 1). The $\delta^{34}S_{sulfate}$ of the paleo fracture fluids is unknown and likely changed over time. However, the $\delta^{34}S_{sulfate}$ values of the current fracture fluids (+14 to +27 ‰: Drake et al., 2013) are similar to the median $\delta^{34}S_{barite}$ values at Forsmark (+26.6 ‰) and Laxemar (+18.3 ‰), suggesting dissolved sulfate in such fluids is a plausible source for barite. The total range of $\delta^{34}S_{barite}$ (+7.6 to +52.0 ‰) is consistent with processing of such fracture fluids by MSR under closed system conditions (Paytan et al., 2002). However, this range is much narrower than that of $\delta^{34}S_{pyrite}$ (−53.9 to +131.7 ‰) across Forsmark and Laxemar (Figs. 2,3; Table 1). Thus, the ancient barite from Forsmark and Laxemar does not record the extreme ^{34}S-enrichment expected from the $\delta^{34}S_{pyrite}$ data. This agrees with barite that recently precipitated on drill core equipment within a deep borehole at Äspö (Fichtner et al., 2024), and carbonate-associated sulfate from the Forsmark and Laxemar drill cores (Fichtner et al., 2026). Therefore, a record of extremely ^{34}S-enriched sulfate in the deep subsurface remains undetected.

Table 1: Stable isotope data ($\delta^{34}S$, $\delta^{18}O$, $\delta^{13}C$) of fracture-hosted minerals (barite, pyrite, calcite) from Forsmark and Laxemar (Fennoscandian Shield, Sweden). Barite data were analyzed in this study. Calcite and pyrite data were obtained from Drake et al. (2017, 2018).

	$\delta^{34}S_{barite}$ (‰, V-CDT)	$\delta^{18}O_{barite}$ (‰, V-SMOW)	$\delta^{34}S_{pyrite}$ (‰, V-CDT)	$\delta^{13}C_{calcite}$ (‰, V-PDB)	$\delta^{18}O_{calcite}$ (‰, V-SMOW)
Forsmark					
n	25	22	793	585	603
Min	+16.5	−0.9	−42.4	−70.3	+13.4
Max	+36.8	+16.9	+65.8	+36.5	+30.9
Average	+28.0	+12.4	+13.8	−10.8	+18.8
Median	+26.6	+15.1	+13.2	−11.8	+18.8
SD	7.3	5.0	16.5	17.2	2.6
Laxemar					
n	480	350	874	621	487
Min	+7.6	+3.1	−53.9	−93.1	+10.5
Max	+52.0	+19.7	+131.7	+7.1	+28.1
Average	+19.5	+12.3	+32.3	−16.5	+20.3
Median	+18.3	+12.3	+23.3	−9.6	+21.0
SD	6.7	3.0	43.8	19.7	3.4

hat gelöscht: compiled
hat gelöscht: published microscale
hat gelöscht: ,
hat gelöscht: data from
hat gelöscht: with new SIMS $\delta^{18}O_{barite}$ and $\delta^{34}S_{barite}$ and analyses from Forsmark and Laxemar (
hat gelöscht: , Figs. 2-3).
hat gelöscht: ¶
hat gelöscht: 21
hat gelöscht: 17.2
hat gelöscht: 28.1
hat gelöscht: 29.7
hat gelöscht: 34.5
hat gelöscht: 1σ
hat gelöscht: 6.5
hat gelöscht: .4
hat gelöscht: 5
hat gelöscht: 323
hat gelöscht: 209
hat gelöscht: 728
hat gelöscht: 352
hat gelöscht: 259
hat gelöscht: 1σ
hat gelöscht: ¶
... [10]

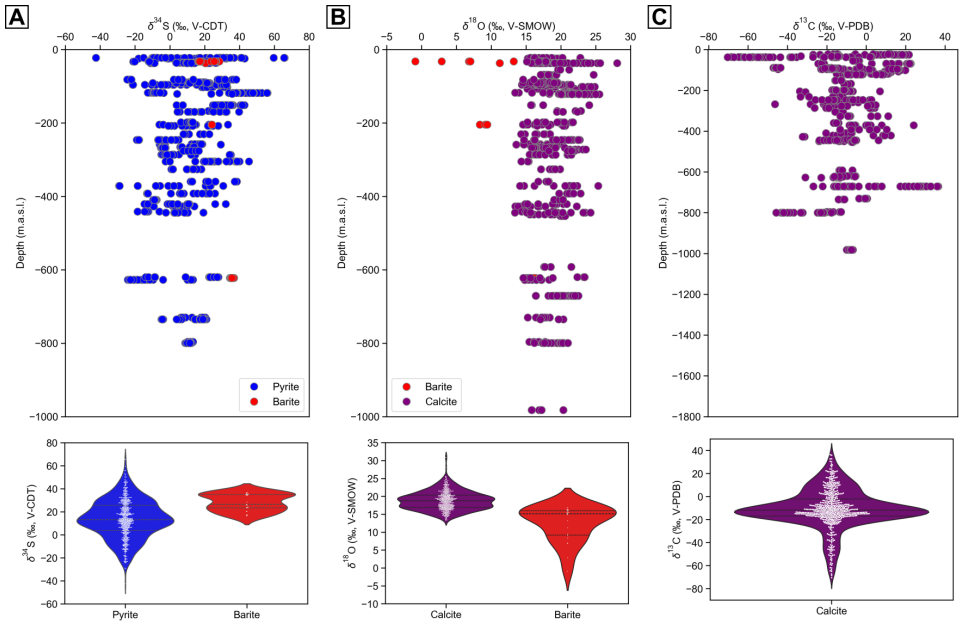


Figure 2: Depth distribution and violin plots of stable isotope data for fracture-hosted minerals from Forsmark. A: $\delta^{34}S_{barite}$, $\delta^{34}S_{pyrite}$, B: $\delta^{18}O_{barite}$, $\delta^{18}O_{calcite}$. The $\delta^{18}O_{calcite}$ data were converted from V-PDB to V-SMOW for comparison with $\delta^{18}O_{barite}$. C: $\delta^{13}C_{calcite}$. Each datapoint represents one SIMS analysis spot (m.a.s.l. = meters above sea level). Barite data were analyzed in this study. Calcite and pyrite were obtained from Drake et al. (2017, 2018).

hat gelöscht: (

hat gelöscht: ,

hat gelöscht: , and

hat gelöscht:) for fracture-hosted minerals from Forsmark.

hat verschoben (Einfügung) [2]

hat gelöscht: spot

hat gelöscht: measurement

hat gelöscht: ,

hat gelöscht: , and barite data

hat gelöscht: . $\delta^{18}O_{calcite}$ data were converted from V-PDB to V-SMOW for comparison with $\delta^{18}O_{barite}$.

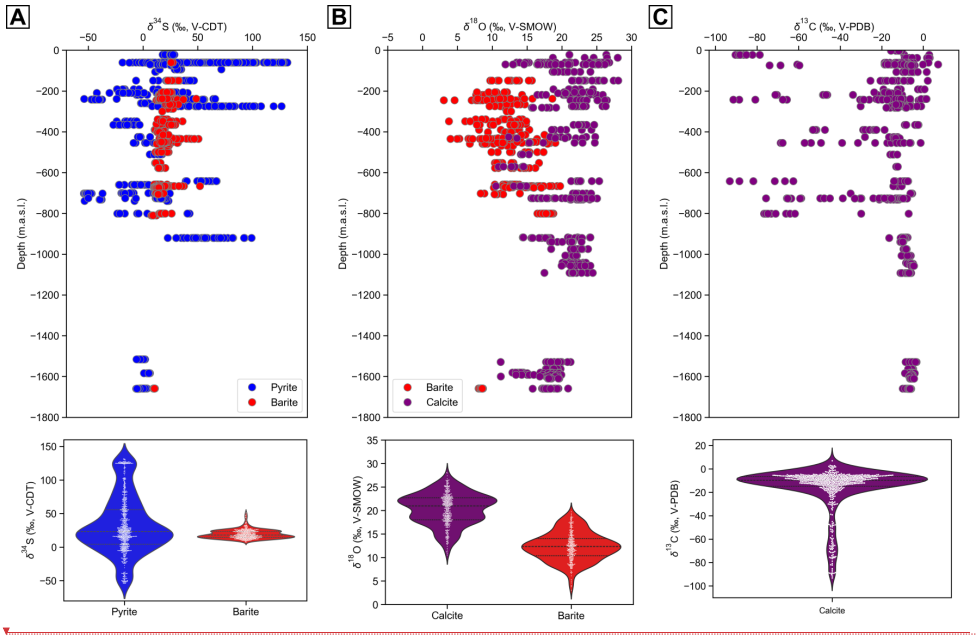
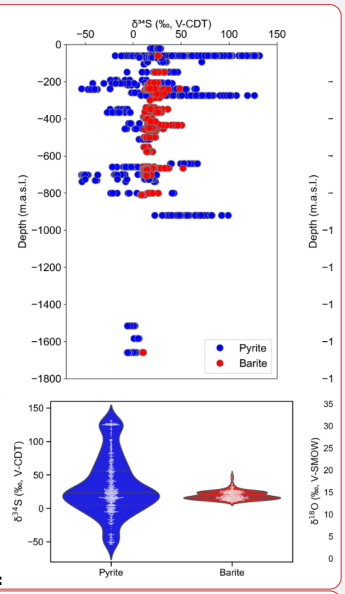


Figure 3: Depth distribution and violin plots of stable isotope data for fracture-hosted minerals from Laxemar. A: $\delta^{34}S_{barite}$, $\delta^{34}S_{pyrite}$. B: $\delta^{18}O_{barite}$, $\delta^{18}O_{calcite}$. The $\delta^{18}O_{calcite}$ data were converted from V-PDB to V-SMOW for comparison with $\delta^{18}O_{barite}$. C: $\delta^{13}C_{calcite}$. Each datapoint represents one SIMS analysis spot (m.a.s.l. = meters above sea level). Barite data were analyzed in this study. Calcite and pyrite were obtained from Drake et al. (2017, 2018).

3.2 Variable sulfate reduction rates and pathways explain microscale $\delta^{18}O$-$\delta^{34}S$-$\delta^{13}C$ data

The co-variation of the $\delta^{18}O_{barite}$ and $\delta^{34}S_{barite}$ values exhibited substantial scatter (Fig. 4a), implying a mixture of different sulfate sources and/or an overlap of different fractionation processes. Since the $\delta^{18}O/\delta^{34}S$ systematics of dissolved sulfate in the low-temperature groundwater systems at Forsmark and Laxemar are affected by OSR and AOM (Drake et al., 2017, 2018; Fichtner et al., 2024), we aimed at identifying whether our dataset contains groups of barite associated with either OSR or AOM. To identify barite associated with these groups, we classified our dataset using Gaussian Mixture Modelling (GMM) and compared the linear regression slopes of the resulting clusters with known sulfate $\delta^{18}O/\delta^{34}S$ trends in MSR-affected settings. We identified a steeper trending 'Group 1' cluster (slope: 0.96 ± 0.01; r^2 = 0.37) and a shallower trending 'Group 2' cluster (slope: 0.55 ± 0.01; r^2 = 0.40) (Fig. 4a; Table 2). The clusters resulting from GMM are statistical entities and cannot be interpreted as continuous fractionation trends in our study. This is because our dataset contains multiple barite growth generations from different locations and records different fractionation trends, non-coeval sulfate reservoirs between growth



hat gelöscht:
hat gelöscht: (
hat gelöscht: ,
hat gelöscht: , and
hat gelöscht:) of fracture-hosted minerals from Laxemar.
hat gelöscht: represents one SIMS measurement
hat gelöscht: ,
hat gelöscht: , and barite data
hat gelöscht: . $\delta^{18}O_{calcite}$ data were converted from V-PDB to V-SMOW for comparison with $\delta^{18}O_{barite}$.
hat gelöscht: 1 Absence of extremely ^{34}S-enriched barite¶ In Forsmark, $\delta^{34}S_{barite}$ ranged from +17.
hat gelöscht: to +36.8 ‰ (median = +34.5 ‰; n = 21), and $\delta^{18}O_{barite}$ ranged from −0.9 to +16.9 ‰ (median = +15.1‰ ... [11]
hat gelöscht: in such fluids is a plausible sulfur source for barite and pyrite. The total range of $\delta^{34}S_{barite}$ (+7.6 to +52 ... [12]
hat gelöscht: due to absence of pyrite, making it difficult to establish the relationship between barite and pyrite. Rega ... [13]
hat gelöscht: 3.2 Microbial sulfur cycling recorded in ancient
hat gelöscht: in
hat gelöscht: follows two distinct trends (Fig. 4a). We applied a
hat gelöscht: to discriminate our $\delta^{18}O_{barite}$ and $\delta^{34}S_{barite}$ data into two groups (Fig. 4b), which are hereafter referred to as 'Gro ... [14]
hat gelöscht: yielded
hat gelöscht: 0.93 (R^2= 0.49) and 0.48 (R^2=0.80) for the Group 1 and Group 2 trends, respectively (Fig. 4b). The poor R^2 valu ... [15]
hat gelöscht: . Thus, each of the two groups reflects multiple fractionation processes occurring in separate fractures and at ... [16]

zones, or local fluid mixing. Therefore, our statistical analysis can only detect average $\delta^{18}O/\delta^{34}S$ trends of overlapping fractionation or mixing processes involving fracture water sulfate that was processed by OSR and AOM at different points in space and time. These overlapping trends likely explain the low r^2 values. There was no correlation between Group 1 and Group 2 barite and the $\delta^{18}O$ values of co-genetic calcite (Fig. 4b). This suggests that the difference between Group 1 and Group 2 does not simply reflect isotopically distinct water sources (Pedersen et al., 1997). Instead, they most likely record different processes affecting the respective sulfate reservoirs from which barite precipitated.

Previous studies established a control of sulfate reduction rates (SRR) during the early stages of MSR on the $\delta^{18}O/\ \delta^{34}S$ slope in residual sulfate (Brunner et al., 2005; Han et al., 2025; Wortmann et al., 2007). At a lower SRR, $\delta^{18}O$ rises rapidly relative to $\delta^{34}S$ leading to a steeper slope, whereas at a higher SRR, $\delta^{18}O$ rises slowly relative to $\delta^{34}S$, leading to a shallower slope (Fig. 1). Thus, the difference in $\delta^{18}O/\delta^{34}S$ slopes could reflect a lower SRR in Group 1 than in Group 2 barite (Fig. 4a). Moreover, differences in metabolic pathways (OSR vs. AOM) can lead to variable $\delta^{18}O/\delta^{34}S$ trends in sulfate at similar SRR (Antler et al., 2013, 2014, 2015). To clarify the effects SRR and MSR pathways on $\delta^{18}O/\delta^{34}S$ systematics recorded in barite at Forsmark and Laxemar, we correlated our GMM-classified $\delta^{18}O_{barite}$ and $\delta^{34}S_{barite}$ data (i.e., excluding outliers) with the $\delta^{13}C$ values of calcite in the same samples (Figs. 2c,3c,4c). When petrographic correlation of barite with individual calcite generations was not possible, we used average $\delta^{13}C_{calcite}$ values from the barite-bearing samples. Out of all classified barite data, 71 spots in Group 1 and 79 spots in Group 2 had associated $\delta^{13}C_{calcite}$ data. Strongly ^{13}C-depleted calcite ($\delta^{13}C \leq -40$ ‰) was almost exclusively associated with Group 1 barite (27 out of 71) (Fig. 4c). The $\delta^{13}C$ values of this calcite (−70 to −40 ‰) cannot be explained by oxidation of organic matter via OSR alone and suggest variable input of inorganic C from the oxidation of primarily microbial methane (Drake et al., 2015, 2017). This implies that some Group 1 barite associated with such calcite was affected by AOM. In contrast, only 2 out of 79 spots in Group 2 barite were associated with strongly ^{13}C-depleted calcite. Instead, Group 2 was almost exclusively associated with calcite that has a $\delta^{13}C \approx -30$ ‰ or higher (Fig. 4c), suggesting methane was not the main C source (Whiticar, 1999). This calcite likely reflects a more prominent contribution from organic matter rather than methane oxidation, implying that the associated barite was affected by OSR (Drake et al., 2017). Notably, such OSR-related barite not only dominates Group 2, but also widely occurs in the AOM-affected Group 1 (Fig. 4c). Thus, it seems unlikely that the different MSR pathways are the only control on the different slopes of both groups. Instead, we interpret the different $\delta^{18}O/\delta^{34}S$ trends to result from an interplay of MSR pathways and SRR: Group 1 reflects AOM and OSR at a relatively low SRR, whereas Group 2 dominantly reflects OSR at a relatively high SRR.

Table 2: Statistical parameters of the groups resulting from the Gaussian Mixture Model.

	Min	Max	Median	Average	SD
Group 1 (n=221)					
$\delta^{34}S_{barite}$ (‰, V-CDT)	+9.4	+23.2	+15.1	+15.2	3.0
$\delta^{18}O_{barite}$ (‰, V-SMOW)	+6.8	+18.8	+12.8	+12.7	2.8
Group 2 (n=123)					

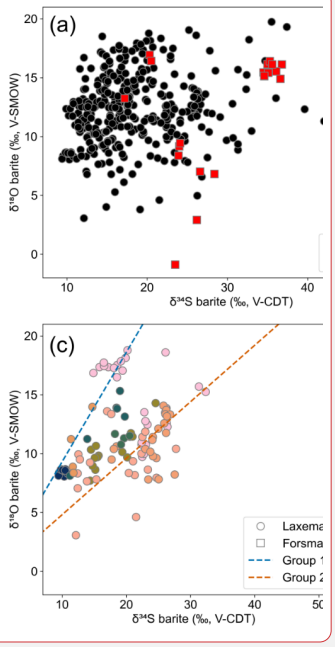
hat gelöscht: 4c…b). This suggests that the trends observed in barite do not correspond to different environments with specific hydrogeochemical regimes…ifference between Group 1 and Group 2 does not simply reflect isotopically distinct water sources (Pedersen et al., 1997). Instead, they most likely record different processes affecting the respective sulfate reservoirs during…rom which barite formation. … [17]

hat gelöscht: Ancient microbial sulfur cycling in deep subsurface fractures at Forsmark and Laxemar was demonstrated by coupled $\delta^{34}S_{pyrite}$ and $\delta^{13}C_{calcite}$ signatures of organoclastic sulfate reduction (OSR) and sulfate-dependent anaerobic oxidation of methane (AOM) . A prominent role of thermochemical sulfate reduction (TSR) in these localities has been ruled out because of the large degree of fractionation between plausible $\delta^{34}S_{SO4}$…To clarify the effects SRR and MSR pathways on $\delta^{18}O/\delta^{34}S$ systematics recorded in barite at Forsmark and Laxemar, we correlated our GMM-classified $\delta^{18}O_{barite}$ and $\delta^{34}S_{barite}$ data (i.e., excluding outliers) with the $\delta^{13}C$ value … [18]

hat gelöscht: the …verage $\delta^{13}C_{calcite}$ values from the barite-bearing samples. Out of all classified barite data, 71 spots in Group 1 and 79 spots in Group 2 had associated $\delta^{13}C_{calcite}$ data. Strongly ^{13}C-depleted calcite ($\delta^{13}C \approx -70$ to… −40 ‰) was almost exclusively associated with Group 1 barite (Fig. 4d). Such strong ^{13}C-depletion as −70‰ suggests anaerobic…7 out of 71) (Fig. 4c). The $\delta^{13}C$ values of this calcite (−70 to −40 ‰) cannot be explained by oxidation of organic matter via OSR alone and suggest variable input of inorganic C from the oxidation of primarily microbial methane (Drake et al., 2015, 2017)with limited input from other carbon sources … Howe … [19]

hat gelöscht: predominantly

hat verschoben (Einfügung) [3]



hat gelöscht:

$\delta^{34}S_{barite}$ (‰, V-CDT)	+14.9	+36.8	+24.2	+24.2	5.0
$\delta^{18}O_{barite}$ (‰, V-SMOW)	+4.0	+16.4	+11.5	+11.5	2.7
Outliers (n=22)					
$\delta^{34}S_{barite}$ (‰, V-CDT)	+12.1	+52.0	+35.8	+34.7	11.4
$\delta^{18}O_{barite}$ (‰, V-SMOW)	−0.9	+19.7	+13.2	+12.2	6.4

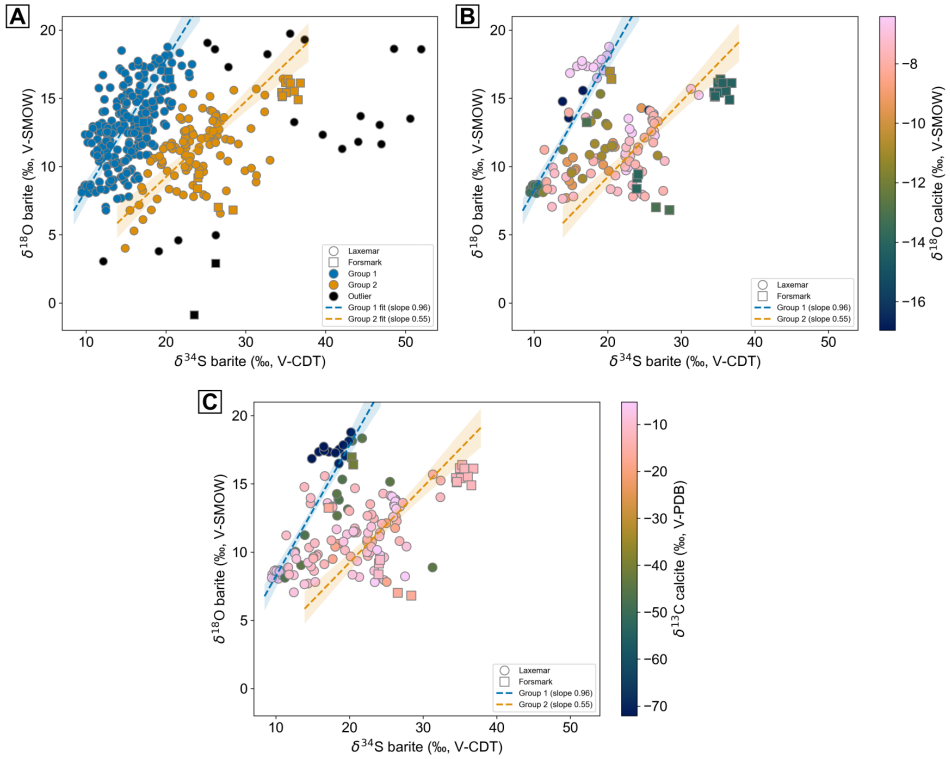


Figure 4: Gaussian Mixture Modelling (GMM) of barite $\delta^{18}O$-$\delta^{34}S$ data and correlation with published calcite δ18O-δ13C data. Each datapoint represents one spot with paired SIMS $\delta^{18}O$ and $\delta^{34}S$ analyses. (a) $\delta^{18}O$ and $\delta^{34}S$ analyses of barite and GMM derived cluster assignments of datapoints. The two-component GMM of barite $\delta^{18}O$ and $\delta^{34}S$ data after exclusion of outliers (black) yielded 'Group 1' and 'Group 2' barite. York regression yielded slopes of 0.96 for Group 1 and 0.55 for Group 2. The range of the regression

hat gelöscht: Stable isotope cross plots and
hat gelöscht: and
hat gelöscht: vs.
hat gelöscht: and
hat gelöscht: spot
hat gelöscht: analysis.
hat gelöscht: . (b)
hat gelöscht: using two cluster centers, yielding
hat gelöscht: barite
hat gelöscht: Major axis
hat gelöscht: of both groups revealed
hat gelöscht: 93
hat gelöscht: 48, respectively. (c

lines equals the data range used for GMM and hence cannot be extended to the outliers. For details on the statistical methodology and its validation, see the Supplementary Materials. (b) $\delta^{18}O$ and $\delta^{34}S$ analyses of barite color-coded by $\delta^{18}O$ of calcite in the same sample. There was no apparent correlation between the Group 1 and Group 2 trends and their corresponding $\delta^{18}O_{calcite}$ values, demonstrating that the trends arise from fractionation processes affecting the sulfate reservoir, rather than fluid mixing. (c) $\delta^{18}O$ and $\delta^{34}S$ analyses of barite color-coded by $\delta^{13}C_{calcite}$ in the same sample. The $\delta^{13}C_{calcite}$ data suggest that AOM barite occurs almost exclusively in Group 1. In contrast, OSR-related barite occurred in Groups 1 and 2. Note that the AOM-related Group 1 barite follows a steeper trend than the OSR-dominated Group 2, contrary to observations by Antler et al. (2014). The color coding in (b) & (c) follows recommendations for scientifically derived color maps (Crameri et al., 2020).

3.3 Hydrogeochemical controls on sulfate reduction rates and pathways

The major control on SRR is the availability and quality of electron donors (i.e., H_2, CH_4, or organic matter) (Leavitt et al., 2013; Lyons and Gaudette, 1979; Westrich and Berner, 1984). SRR is high when electron donors are more bioavailable and abundant vice versa. The abundance of electron donors in the parent fluids from which our ancient barite precipitated are unknown. However, low SRR due to nutrient limitation was inferred based on the large apparent $^{34}\varepsilon$ associated with pyrite formation at these sites (Drake et al., 2018), consistent with the common free energy limitation in deep subsurface habitats in general (Hoehler and Jørgensen, 2013). Thus, a relatively lower availability of electron donors in Group 1 could have caused the lower inferred SRR than in Group 2 (Fig. 5a). Moreover, the typical range of sulfate concentrations in modern anoxic fracture fluids at Forsmark and Laxemar (<1 to 10 mM: Hallbeck & Pedersen, 2008; Laaksoharju et al., 2008; Drake et al., 2013) is much lower than in marine environments (28 mM in seawater: Jørgensen et al., 2019). Such sulfate concentrations may additionally limit SRR in the deep subsurface (Boudreau and Westrich, 1984; Pallud and Van Cappellen, 2006). Sulfate concentrations in these subsurface habitats also vary around the threshold at which sulfate reducers outcompete methanogens for substrate utilization (ca. 1-10 mM) (Iversen & Jorgensen, 1985; Glossner et al., 2016; Sela-Adler et al., 2017). If sulfate concentrations exceed this threshold, OSR can be favored, inhibiting methanogenesis and AOM. Thus, $\delta^{13}C$ evidence for AOM indirectly supports sulfate limitation in Group 1 (Fig. 4c). Thus, a combined effect of electron donor limitation and low sulfate concentrations could have favored methanogenesis and AOM at relatively low SRR (Fig. 5a). Conversely, a higher abundance of electron donors could explain a higher inferred SRR in Group 2 than in Group 1 (Fig. 5b). At higher sulfate availability, methanogenesis is inhibited, possibly resulting in the lack of evidence for AOM in Group 2 (Fig. 5b). Instead, OSR is favored and SRR is high, resulting in a shallower trend in Group 2 (Fig. 5b). Thus, we interpret the relative abundances of sulfate and electron donors to control the observed $\delta^{18}O/\delta^{34}S$ trends in ancient subsurface barite by modulating SRR and MSR pathways. The stronger ^{34}S-enrichment in the OSR-dominated Group 2 than in the AOM-affected Group 1 contrasts with observations from marine sediments, where ^{34}S-enriched barite is a commonly used proxy for AOM at the SMTZ (Torres et al., 1996; Wood et al., 2021; Yang et al., 2023; Zan et al., 2022; Zhou et al., 2015). This discrepancy is possibly due to the higher sulfate concentration in seawater (28 mM: Jørgensen et al., 2019) compared to the subsurface at Forsmark and Laxemar (<1 to 10 mM), allowing sulfate to become strongly ^{34}S-enriched before barite becomes undersaturated (Fichtner et al., 2024). The relatively steep slope of the AOM-affected Group 1 is comparable to some previous observations from marine methane-diffusion-limited AOM settings, such as sedimentary SMTZs, or OSR-dominated methane-devoid settings (Antler et al., 2013, 2015; Blake et al., 2006; Böttcher et al., 2006). At the same time, Group 2 shows little clear evidence of AOM but a shallow

hat gelöscht: Note that there were no samples from Forsmark with coupled $\delta^{18}O_{barite}$-$\delta^{34}S_{barite}$-$\delta^{13}C_{calcite}$ data. (d

hat gelöscht:) & (d

hat gelöscht: Controls

hat gelöscht: $\delta^{18}O$/ $\delta^{34}S$ trends in barite: pathways versus rates of microbial

hat verschoben (Einfügung) [4]

slope similar to marine methane-in-excess environments (i.e., the methane flux exceeds methane consumption via oxidation), such as cold seeps (Aharon and Fu, 2000, 2003; Antler et al., 2013, 2014; Rubin-Blum et al., 2014). These observations highlight a further discrepancy between marine environments and the deep subsurface. In marine environments, steeper $\delta^{18}O/\delta^{34}S$ slopes tend to be found in settings affected by OSR or methane-limited AOM, whereas shallower slopes result from AOM at high methane concentrations. In our subsurface barite, steeper slopes tend to be more associated with evidence for AOM, whereas shallower slopes tend to occur in OSR-dominated settings. The relatively shallow slope of OSR-related barite in the subsurface implies a lesser extent of equilibrium isotope exchange of S intermediates with water compared to marine settings. This could be achieved via a higher overall SRR in the subsurface than in marine settings; however, this seems unlikely given the oligotrophic nature of subsurface habitats (Küsel and Dopson, 2026). Additional factors influencing the different behavior of $\delta^{18}O/\delta^{34}S$ trends in the deep subsurface may be the increasing temperature and pressure with depth or factors within microbial communities, such as low cell densities or adaptations to extreme nutrient limitation. However, the impact of these factors on $\delta^{18}O/\delta^{34}S$ relationships in residual sulfate during MSR remains speculative. Irrespective of this unresolved problem, the differences in $\delta^{18}O/\delta^{34}S$ systematics between marine and subsurface barite highlight that interpretations cannot be extended from one system to the other without additional constraints.

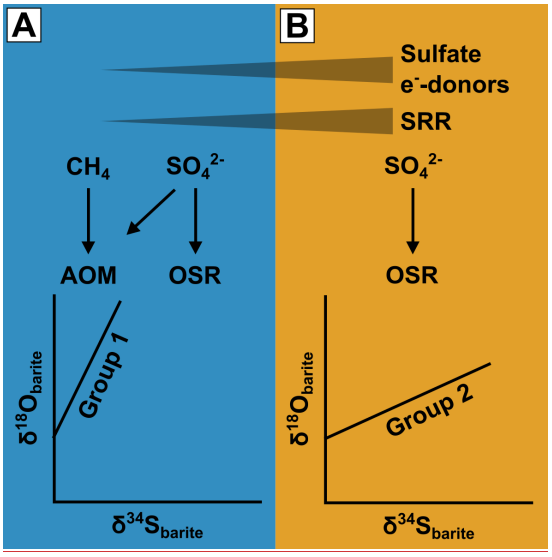


Figure 5: Conceptual model of the controls on $\delta^{18}O_{barite}$ and $\delta^{34}S_{barite}$ systematics in the continental deep subsurface. (a) at low sulfate and electron donor abundances, microbial methanogenesis occurs and microbial sulfate reduction proceeds via both sulfate-dependent anaerobic oxidation of methane (AOM) and organotrophic sulfate reduction (OSR) at a relatively low sulfate reduction rate (SRR). This results in the steep $\delta^{18}O_{barite}/\delta^{34}S_{barite}$ trend recorded in Group 1 barite. (b) at a higher sulfate and electron donor

hat nach oben verschoben [3]: **Table 2: Statistical parameters of the groups resulting from the Gaussian Mixture Model.** ¶

hat verschoben (Einfügung) [5]

hat gelöscht: We found a steeper $\delta^{18}O/\delta^{34}S$ trend in the AOM-affected Group 1 than in the OSR-dominated Group 2 (Fig. 4d). A steeper $\delta^{18}O/\delta^{34}S$ trend suggests a higher degree of sulfur-intermediate re-oxidation relative to sulfate reduction . The relationship between sulfur-intermediate re-oxidation relative to sulfate reduction during the early stages of MSR can be controlled by different metabolic processes (OSR vs. AOM) and sulfate reduction rates (SRR) . The slope of the Group 1 trend matches previous observations from methane-limited AOM settings , consistent with our $\delta^{13}C_{calcite}$ evidence for AOM in Group 1 (Fig. 4d). Thus, our combined $\delta^{18}O_{barite}$, $\delta^{34}S_{barite}$, and $\delta^{13}C_{calcite}$ data may record AOM under methane-limited conditions in Group 1. However, several data points in Group 1 did not show evidence of AOM. Additionally, the trend of the OSR-dominated Group 2 is much shallower than OSR-associated trends previously observed in sedimentary environments (Fig. 4d) . Thus, the variation of $\delta^{18}O_{barite}/\delta^{34}S_{barite}$ trends at Forsmark and Laxemar is apparently not only controlled by the co-occurrence of different metabolic processes.¶
The variability of $\delta^{18}O/\delta^{34}S$ trends in OSR-associated barite may thus be interpreted as a lower SRR in Group 1 than in Group 2 (Fig. 4). Notably, the largest ^{34}S enrichment occurs in the OSR-dominated Group 2 (+12.1 to +52.0 ‰; median = +25.3 ‰; Table 2, Fig. 4b), implying a large apparent $^{34}\varepsilon$. The major control on SRR and $^{34}\varepsilon$ is the balance between the availability of sulfate and electron donors . If the sulfate supply is low relative to that of electron donors, sulfate consumption is rapid and quantitative, while $^{34}\varepsilon$ is diminished. In contrast, if the sulfate supply is high and the electron donor supply is limited, SRR is low, and $^{34}\varepsilon$ is high. Hence, variations in SRR observed in relatively sulfate-rich marine sediments (28 mM in seawater: are generally controlled by the availability of organic substrates . However, the typical range of sulfate concentrations in modern anoxic fracture fluids at Forsmark and Laxemar is 1-10 mM (, implying a more rate-limiting function for sulfate availability in the deep subsurface. ¶
Relatively low sulfate availability in Group 1 is supported by associated $\delta^{13}C$ evidence for AOM (Fig. 4d). In aquatic systems, AOM is favored at the sulfate-methane transition zone (SMTZ) where upward-diffusing methane produced by methanogens meets downward-diffusing sulfate . Thus, the evidence for AOM in Group 1 requires both a methane and a sulfate source for the fracture environment. Substantial methanogenesis is typically only observed below and within the (SMTZ) (. This is because sulfate reducers generally outcompete methanogens for substrate utilization above sulfate concentrations of (~1-10 mM) (. Therefore, if sulfate concentrations exceed this threshold, methanogenesis and AOM may be inhibited. Instead, sulfate reduction may then dominantly proceed via OSR. Thus, a lower sulfate availability may plausibly explain both the evidence for AOM and a lower SRR in Group 1, whereas a higher sulfate availability may explain the predominance of OSR and higher SRR in Group 2.¶
Notably, the trend of our OSR-associated Group 2 is shallower than previously observed OSR-related sulfate in marine environments . It seems unlikely that this can be explained by higher SRR than in marine sediments. The deep continental subsurface is a dominantly oligotrophic environment , suggesting a generally low availability of electron donors for sulfate reduction. Indeed, current fracture fluids at Forsmark and Laxemar/Äspö show low dissolved organic carbon contents (<0.2 mM: . This organic carbon is also highly refra ... [20]

abundance, microbial methanogenesis is inhibited, and MSR proceeds predominantly via OSR at relatively high SRR. This results in the shallow $\delta^{18}O_{barite}$/ $\delta^{34}S_{barite}$ trend recorded in Group 2.

3.4 Barite and pyrite record distinct hydrogeochemical regimes

. This suggests that the mechanism limiting the precipitation of extremely ^{34}S-enriched sulfate is more likely associated with the S cycle, rather than cation availability. Sampling biases cannot be excluded but have been mitigated by the large number of $\delta^{34}S$ analyses (n = 505) of barite from multiple fractures at two localities. Notably, the strongest ^{34}S-enrichment observed here occurs in the outlier group and is not associated with cogenetic calcite data (Fig. 4a-c; Table 2). This makes an interpretation on the associated MSR pathway and SRR difficult for these cases. However, it seems likely that these barites represent relatively late-stage precipitates that possibly formed in an environment where barite saturation was less limiting.

Microscale observations of pyrite-calcite-barite assemblages could help investigating this interpretation further (Figs. 6,7). Sample KAS02 (802 m) can serve as an example of AOM-associated barite due its association with calcite that has an average $\delta^{13}C$ of −72.1 ‰ and pyrite with $\delta^{34}S$ values spanning −23.5 to +42.5 ‰ (Fig. 6a,b). Additionally, all SIMS spots on barite in this sample belong to Group 1 (Fig. 7a). Together, these observations are consistent with a sulfate pool affected by AOM at relatively low SRR. Notably, this barite exhibited distinct crystallographic and isotopic zonation with only minor $\delta^{34}S$ and $\delta^{18}O$ variabilities between growth zones of ~4 and ~0.8 ‰, respectively (Fig. 7a). This low variability suggests relatively open system conditions during barite growth (Fichtner et al., 2024; Wood et al., 2021). In contrast, the much more pronounced core-to-rim $\delta^{34}S$ increase in the co-genetic pyrite from −23.5 to +42.5 ‰ indicates MSR in a more closed system, meaning that SRR exceeded the resupply of sulfate during pyrite growth (Fig. 7a). Apparently, barite and pyrite in this sample record precipitation in distinct hydrogeochemical regimes, possibly at different stages of fracture fluid evolution or in separate microenvironments.

Sample KLX01 (220 m) serves as an example for OSR-related barite due to its association with calcite lacking a substantial $\delta^{13}C$ depletion (−11.6 ‰) (Fig. 6c,d). Notably, barite in this sample exhibited a massive core and a porous rim (Fig. 7b). These texturally distinct growth zones were associated with a sharp core-to-rim $\delta^{34}S$ and $\delta^{18}O$ increase of ~12 ‰ and ~6 ‰, respectively (Fig. 7b). This sharp increase suggests that barite in the rim precipitated from sulfate that had already undergone ^{34}S-enrichment via sulfate reduction elsewhere in the fracture system (e.g., Drake et al., 2018). Additionally, SIMS spots related to Group 1 predominated in the core, whereas spots related to Group 2 exclusively occurred in the rim (Fig. 7b). This implies that the processing of the respective sulfate reservoirs reflected by core and rim occurred under different SRR and/or MSR pathways. Thus, the distinct textural and isotopic differences demonstrate that the generations reflect two barite precipitation events, rather than continuous barite growth. The porosity in the rim suggests barite dissolution (Fig. 7b), possibly due to undersaturation via rapid sulfate depletion at the high SRR inferred for Group 2 (Fichtner et al., 2024). Thus, a relatively high SRR in a sulfate-poor environment may result in a preservation bias against extremely ^{34}S-enriched barite in deep subsurface environments. Relatively minor core-to-rim $\delta^{34}S$ increase of ca. 0 to 20 ‰ in co-genetic pyrite imply that sulfate did not become strongly depleted during pyrite formation in this microenvironment (Fig. 7b). While there was no evidence for AOM from $\delta^{13}C_{calcite}$ in this sample, it cannot be resolved petrographically whether the calcite and pyrite are co-genetic to the

hat gelöscht: The absence of extreme ^{34}S-enrichment in barite from Forsmark and Laxemar is unexpected considering the corresponding $\delta^{34}S_{pyrite}$ values of up to +131.7 ‰ predicting an even more ^{34}S-enriched sulfate reservoir during pyrite formation. The $\delta^{34}S_{barite}$ values of up to +52.0 ‰ observed here suggest that the SRR at times exceeded the sulfate resupply, decreasing the steady state sulfate concentration (i.e., closed-system conditions). Hence, Rayleigh distillation is locally recorded in subsurface barite, although not to the extreme degree observed in pyrite (Fig. 4). This discrepancy between the barite and pyrite records has been suggested to result from (i) the precipitation of barite and pyrite under separate microenvironmental conditions, involving the isolation of evolved ^{34}S-enriched fluids, or (ii) late-stage barite undersaturation which may inhibit sulfate precipitation or favor its post-formation dissolution before the formation of a ^{34}S-enriched sulfate reservoir (Fichtner et al., 2024, 2026). Barite undersaturation may arise from sulfate depletion at high degrees of Rayleigh distillation (Fic… [21]

hat gelöscht: barite-

hat gelöscht: support an interplay of MSR pathways and … [22]

hat gelöscht: 5,6). Barite in sample

hat gelöscht: be taken

hat gelöscht: a prime

hat gelöscht: , it is intergrown

hat gelöscht: ‰, demonstrating an influence of AOM du… [23]

hat gelöscht: the GMM assignment of

hat gelöscht: to the AOM-affected Group 1 (Fig. 5c).

hat gelöscht: core-to-rim

hat gelöscht: increases

hat gelöscht: ‰

hat gelöscht: 5c-e

hat gelöscht: crystallographic and isotopic zonation is co… [24]

hat gelöscht: At the same time, pyrite in this sample displays a

hat gelöscht: of ca. 15

hat gelöscht: 60 ‰ (Fig. 5f), implying

hat gelöscht: high degree of Rayleigh distillation

hat gelöscht: . Thus, Rayleigh distillation during AOM p… [25]

hat gelöscht: formed under different

hat gelöscht: conditions, with pyrite likely recording a la… [26]

hat gelöscht: 6a,b

hat gelöscht: 6c

hat gelöscht: 6c-e

hat gelöscht: .

hat gelöscht: Notably, SIMS spots related to Group 1 … [27]

hat gelöscht: is consistent with

hat gelöscht: , which may have arisen from

hat gelöscht: 6f

barite core or rim. Therefore, it remains unclear whether the shift from Group 1 to Group 2 during barite growth is due to different MSR pathways or SRR, or both. Nevertheless, the differences between the samples KAS02 (802 m) and KLX01 (220 m), as well as their evolution during barite growth, demonstrate a strong control of hydrogeochemical conditions on their isotopic composition in different microenvironments and over time. This highlights that the associated barite and pyrite record different environmental conditions and should be correlated with caution.

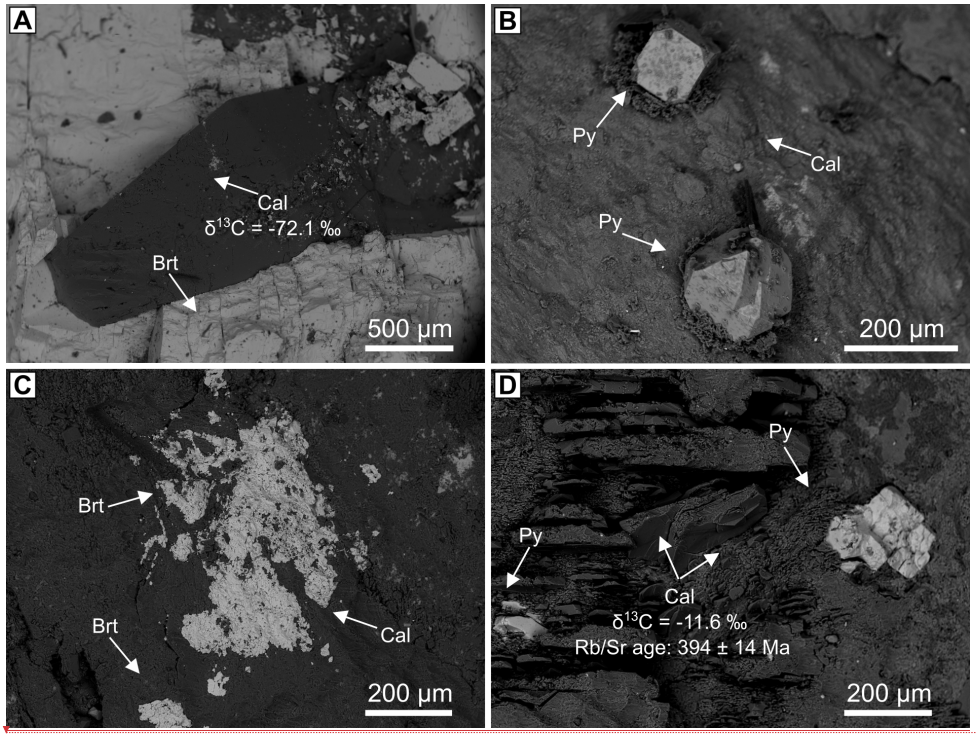
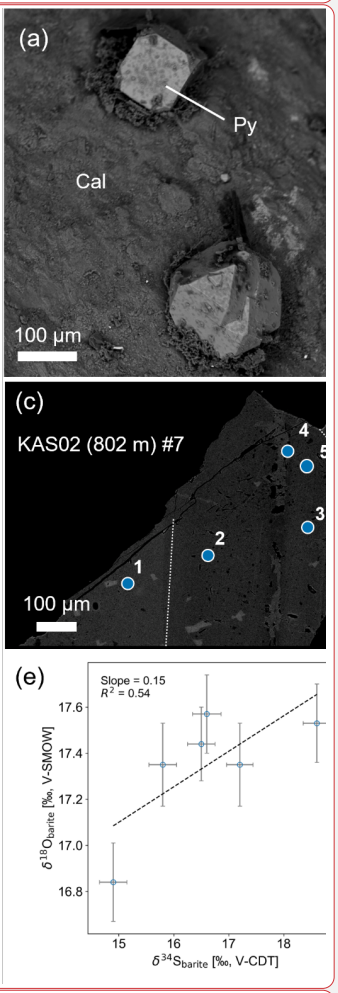


Figure 6: Backscatter electron micrographs of calcite-pyrite-barite assemblages in drill core samples investigated in this study. A-B: Sample KAS2 (802 m depth) from Äspö (i.e., Laxemar). A: Barite (Brt) intergrown with calcite (Cal), demonstrating the coeval formation of barite and calcite. Calcite in this sample has an average $\delta^{13}C$ of −72.1‰, demonstrating calcite precipitation after the oxidation of biogenic methane via AOM (Drake et al., 2017). B: Euhedral pyrite (Py) intergrown with calcite, demonstrating that pyrite is co-genetic with the outermost calcite generation. C-D: Sample KLX1 (220 m depth) from Laxemar. C: Barite intergrown with calcite, demonstrating their co-genetic relationship. D: Pyrite intergrown with calcite, demonstrating the coeval formation of pyrite with calcite and, thus, barite. The calcite generation coeval with barite has a Rb/Sr age of 394 ± 14 Ma and $\delta^{13}C_{calcite}$ = −11.6 ‰ (Drake et al., 2017).

hat gelöscht: . Irrespective of this problem



hat gelöscht:

hat gelöscht: 5: BSE images and stable isotope data…: Backscatter electron micrographs of sample KAS02…alcite-pyrite-barite assemblages in drill core samples investigated in this study. A-B: Sample KAS2 (802 m depth) from Äspö (i.e., Laxemar). (a) Euhedral pyrite (Py) …: Barite (Brt) intergrown with calcite (Cal), demonstrating that pyrite is co-genetic with the outermost calcite generation. (b) Barite (Brt) on the surface of a calcite crystal, demonstrating …he coeval formation of barite calcite. Calcite in this sample has a $\delta^{13}C_{calcite}$…n average $\delta^{13}C$ of −72.1‰, demonstrating calcite precipitation after the oxidation of biogenic methane via AOM (Drake et al., 2017). B: Euhedral pyrite (Py) intergrown with calcite, demonstrating that pyrite is co-genetic with the outermost calcite generation. C-D: Sample KLX1 (220 m depth) from Laxemar. C: Barite intergrown with calcite, demonstrating their co-genetic relationship. D: Pyrite intergrown with calcite, demonstrating the coeval formation of pyrite with calcite and, thus, barite. The calcite generation coeval with barite has a Rb/Sr age of 394 ± 14 Ma and $\delta^{13}C_{calcite}$ = −11.6 ‰ (Drake et al., 2017)(c)

… [28]

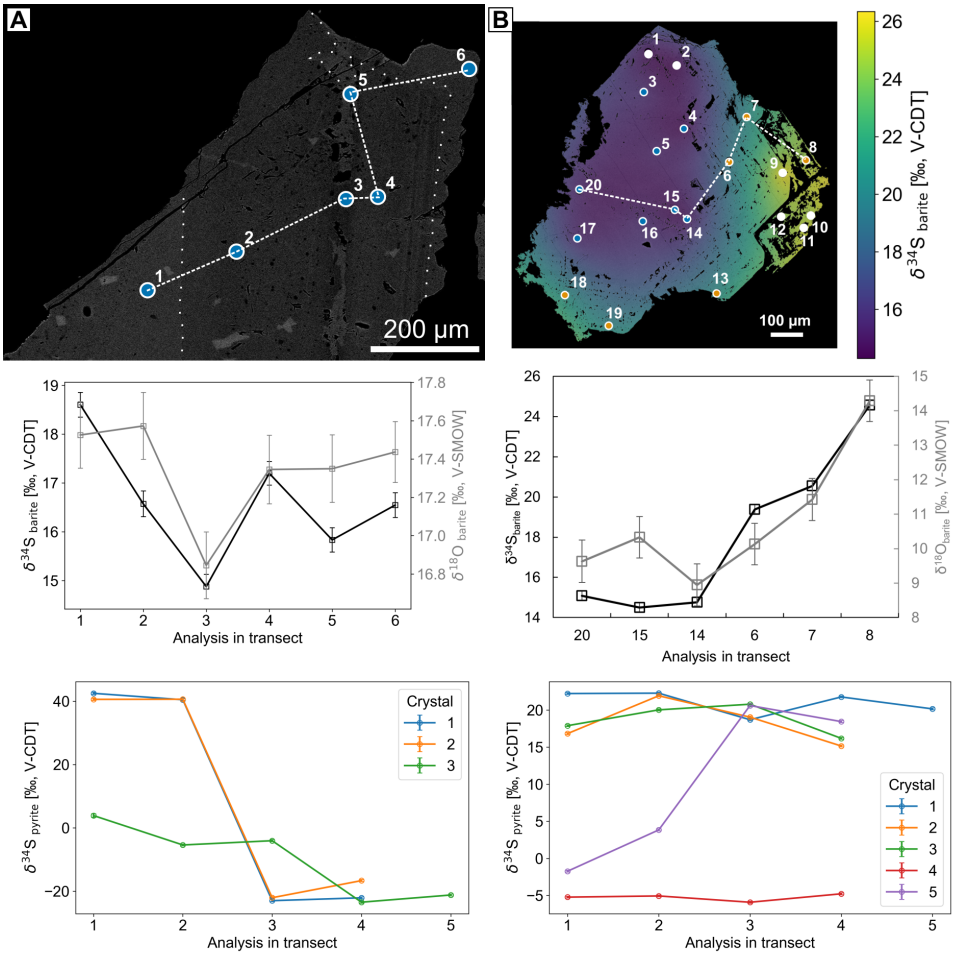


Figure 7: Microscale stable isotope variations in individual barite and pyrite grains. A: SEM image of a polished barite grain with three distinct growth zones and SIMS analytical transects of barite and associated pyrite in sample KAS2 (802 m depth) from Äspö (i.e., Laxemar). The white dotted lines highlight the boundaries between growth zones, whereas the white dashed lines highlight analytical transects. White dots could not be assigned to a group because corresponding $\delta^{18}O_{barite}$ values were lacking. Transects across three pyrite crystals from the same sample show a $\delta^{34}S_{pyrite}$ variation of ca. 65 ‰ across two of the crystals. B: SEM image of a polished barite grain with two distinct growth zones and SIMS analytical transects of barite and associated pyrite in sample KLX1 (220 m depth) from Laxemar. The overlain heatmap was interpolated via cubic convolution and does not reflect measured $\delta^{34}S$

hat gelöscht: crystal showing growth zonation and $\delta^{34}S_{barite}$ and $\delta^{18}O_{barite}$ SIMS spots. The white dashed line highlights the boundary between crystallographic

hat gelöscht: . The color coding of the analysis spots signifies their assignment

hat gelöscht: Group 1 (blue) according to Fig. 3b. (d) Transect

values beyond the analyzed spots. The transect across a zoned barite crystal shows co-variation of $\delta^{34}S_{barite}$ and $\delta^{18}O_{barite}$ with higher ^{34}S- and ^{18}O-enriched values in the later generation (rim). The transect across five pyrite grains from the same sample shows a $\delta^{34}S_{pyrite}$ variation of ca. 20 ‰ across one grain. The color coding of the analysis spots in (A) and (B) reflects their assignment to Group 1 (blue) and Group 2 (orange) according to Fig. 4c. The error bars associated with pyrite analyses are smaller than the symbols.

4 Conclusions

We compiled previously published microscale $\delta^{13}C_{calcite}$, $\delta^{18}O_{calcite}$, and $\delta^{34}S_{pyrite}$ data with new SIMS $\delta^{18}O_{barite}$ and $\delta^{34}S_{barite}$ analyses to investigate biosignature records in ancient deep subsurface mineral assemblages from Forsmark and Laxemar/ Äspö (Southeastern Sweden). We identified two groups of barites recording microbial sulfate reduction (MSR) associated with distinct $\delta^{18}O/\delta^{34}S$ slopes. Comparison with coeval $\delta^{13}C_{calcite}$ data revealed that evidence for sulfate-dependent anaerobic oxidation of methane (AOM) is mostly restricted to the steeper trending Group 1, whereas Group 2 was dominated by organotrophic sulfate reduction (OSR). We interpret the different slopes to result from an interplay of variable sulfate reduction rates (SRR) and MSR pathways (AOM vs. OSR): Group 1 reflects AOM and OSR at relatively low SRR, whereas Group 2 dominantly reflects OSR at relatively high SRR. Variations in SRR and MSR pathways likely reflect the relative sulfate and electron donor abundances in the barites' parent fluids. Barite records $\delta^{34}S$ values up to +52.0 ‰, which is well below the extreme ^{34}S-enrichment observed in some pyrite from the same locality ($\delta^{34}S_{pyrite}$ = +131.7 ‰). The discrepancy between barite and pyrite records could reflect their formation in separate microenvironments or may be due to undersaturation caused by sulfate and/or Ba^{2+} depletion at high degrees of Rayleigh distillation. In concert, microscale C-O-S isotope signatures in fracture-hosted pyrite-calcite-barite assemblages at Forsmark and Laxemar record biosignatures of AOM and OSR deep within the Fennoscandian Shield since at least 394 Ma, but these records are affected by local hydrogeochemical conditions. Signatures of metabolic processes in barite varied over time within the same microenvironment and between different fractures. This highlights that understanding deep subsurface geobiology requires integrated microscale analyses of mineral assemblages distributed over large crustal volumes.

Data availability

All data presented in the manuscript are available in the Supplementary Dataset via the online repository Zenodo (doi:10.5281/zenodo.22041131).

Author contributions

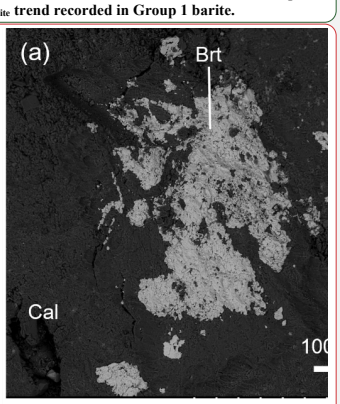
ER: Data curation, Formal analysis, Investigation, Methodology, Validation, Visualization, Writing (original draft preparation), Writing (review and editing). VF: Data curation, Investigation, Formal analysis, Writing (review and editing). MT: Data curation, Investigation, Formal analysis, Writing (review and editing). MW: Resources, Writing (review and

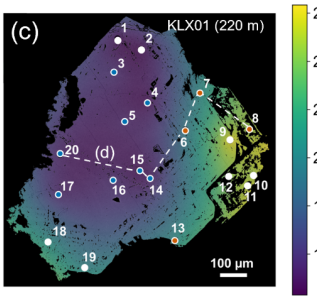
hat gelöscht: in (c) showing…hows co-variation of $\delta^{34}S_{barite}$ and $\delta^{18}O_{barite}$ with higher ^{34}S- and ^{18}O-enriched values in the later generation (rim). (d) $\delta^{34}S_{barite}$ vs $\delta^{18}O_{barite}$ scatter plot showing a slope of 0.15. (f) Transect…he transect across three…ive pyrite grains from the same sample , showing…hows a $\delta^{34}S_{pyrite}$ … [29]

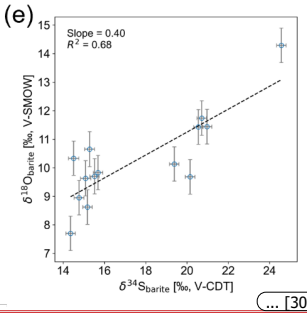
hat nach oben verschoben [4]:). At higher sulfate availability, methanogenesis is inhibited, possibly resulting in the lack of evidence for AOM in Group 2 (Fig.

hat nach unten verschoben [6]: Signatures of metabolic processes in barite varied over time within the same microenvironment and between different fractures.

hat nach oben verschoben [5]: **This results in the steep $\delta^{18}O_{barite}$/ $\delta^{34}S_{barite}$ trend recorded in Group 1 barite.**







hat gelöscht: … [30]

hat gelöscht: 7b). Instead, OSR is favored and SRR is high, resulting in a stronger ^{34}S-enrichment and a shallower trend in Group 2 (Fig. 7b). This ^{34}S-enrichment suggests that the SRR at times exceeded the sulfate resupply, decreasing the steady state sulfate concentration (i.e., closed system conditions). This highlight… [31]

hat gelöscht: Understanding deep subsurface geobiology thus requires microscale analyses distributed over large crustal volumes. Moreover, distinguishing OSR and AOM was aided by tying $\delta^{13}C_{calcite}$ values with trajectories in $\delta^{18}O_{barite}$/ $\delta^{34}S_{barite}$ space. Thus, our study highlights the need for microscale multiple stable isoto… [32]

hat gelöscht: **(b) at a higher sulfate/ electron donor ratio, microbial methanogenesis is inhibited, and MSR proceeds predominantly via OSR at relatively high SRR. This results in the shallow $\delta^{18}O_{barite}$/ $\delta^{34}S_{barite}$ trend recorded in Group 2.**¶

editing). HD: Conceptualization, Funding acquisition, Methodology, Project administration, Resources, Supervision, Writing (review and editing).

Competing interests

The authors declare no competing interests.

Acknowledgements

This work was supported by grants of the Swedish Nuclear Fuel and Waste Management Co. (SKB), Swedish research council (2021-04365, 2025-04466), Formas (2020-01577), J. Gust. Richert foundation (2023-00850), the Crafoord foundation (20210524), and National Science Foundation (2120733) to Henrik Drake. We thank Heejin Jeon for assistance in SIMS sample preparation and analysis and Andrea Göhring for valuable input on our statistical methodology. The AI tool Claude (Anthropic PBC) was used to help generating code for statistical analysis and all generated output has been verified by the authors. This is NordSIMS publication #XXX.

hat gelöscht: .

References

Aharon, P. and Fu, B.: Microbial sulfate reduction rates and sulfur and oxygen isotope fractionations at oil and gas seeps in deepwater Gulf of Mexico, Geochim. Cosmochim. Acta, 64, 233–246, https://doi.org/10.1016/S0016-7037(99)00292-6, 2000.

Aharon, P. and Fu, B.: Sulfur and oxygen isotopes of coeval sulfate–sulfide in pore fluids of cold seep sediments with sharp redox gradients, Chemical Geology, 195, 201–218, https://doi.org/10.1016/S0009-2541(02)00395-9, 2003.

Aloisi, G., Bouloubassi, I., Heijs, S. K., Pancost, R. D., Pierre, C., Sinninghe Damsté, J. S., Gottschal, J. C., Forney, L. J., and Rouchy, J.-M.: CH_4 -consuming microorganisms and the formation of carbonate crusts at cold seeps, Earth Planet. Sci. Lett., 203, 195–203, https://doi.org/10.1016/S0012-821X(02)00878-6, 2002.

Aloisi, G., Wallmann, K., Bollwerk, S. M., Derkachev, A., Bohrmann, G., and Suess, E.: The effect of dissolved barium on biogeochemical processes at cold seeps, Geochim. Cosmochim. Acta, 68, 1735–1748, https://doi.org/10.1016/j.gca.2003.10.010, 2004.

Anderson, T. F., Kruger, J., and Raiswell, R.: C-S-Fe relationships and the isotopic composition of pyrite in the New Albany Shale of the Illinois Basin, U.S.A., Geochim. Cosmochim. Acta, 51, 2795–2805, https://doi.org/10.1016/0016-7037(87)90159-1, 1987.

Antler, G., Turchyn, A. V., Rennie, V., Herut, B., and Sivan, O.: Coupled sulfur and oxygen isotope insight into bacterial sulfate reduction in the natural environment, Geochim. Cosmochim. Acta, 118, 98–117, https://doi.org/10.1016/j.gca.2013.05.005, 2013.

Antler, G., Turchyn, A. V., Herut, B., Davies, A., Rennie, V. C. F., and Sivan, O.: Sulfur and oxygen isotope tracing of sulfate driven anaerobic methane oxidation in estuarine sediments, Estuar. Coast. Shelf Sci., 142, 4–11, https://doi.org/10.1016/j.ecss.2014.03.001, 2014.

Antler, G., Turchyn, A. V., Herut, B., and Sivan, O.: A unique isotopic fingerprint of sulfate-driven anaerobic oxidation of methane, Geology, 43, 619–622, https://doi.org/10.1130/G36688.1, 2015.

Bar-On, Y. M., Phillips, R., and Milo, R.: The biomass distribution on Earth, Proc. Natl. Acad. Sci. U.S.A., 115, 6506–6511, https://doi.org/10.1073/pnas.1711842115, 2018.

Bell, E., Lamminmäki, T., Alneberg, J., Qian, C., Xiong, W., Hettich, R. L., Frutschi, M., and Bernier-Latmani, R.: Active anaerobic methane oxidation and sulfur disproportionation in the deep terrestrial subsurface, ISME J., 16, 1583–1593, https://doi.org/10.1038/s41396-022-01207-w, 2022.

Blake, R. E., Surkov, A. V., Böttcher, M. E., Ferdelman, T. G., and Jørgensen, B. B.: Oxygen isotope composition of dissolved sulfate in deep-sea sediments: Eastern Equatorial Pacific Ocean, in: Proceedings of the Ocean Drilling Program, 201 Scientific Results, vol. 201, edited by: Jørgensen, B. B., D'Hondt, S. L., and Miller, D. J., Ocean Drilling Program, https://doi.org/10.2973/odp.proc.sr.201.116.2006, 2006.

Böttcher, M. E., Bernasconi, S. M., and Brumsack, H.-J.: Carbon, sulfur, and oxygen isotope geochemistry of interstitial waters from the Western Mediterranean, in: Proceedings of the Ocean Drilling Program, 161 Scientific Results, vol. 161, edited by: Zahn, R., Comas, M. C., and Klaus, A., Ocean Drilling Program, https://doi.org/10.2973/odp.proc.sr.161.1999, 1999.

Böttcher, M. E., Ferdelman, T. G., Jørgensen, B. B., Blake, R. E., Surkov, A. V., and Claypool, G. E.: Sulfur isotope fractionation by the deep biosphere within sediments of the Eastern Equatorial Pacific and Peru Margin, in: Proceedings of the Ocean Drilling Program, 201 Scientific Results, vol. 201, edited by: Jørgensen, B. B., D'Hondt, S. L., and Miller, D. J., Ocean Drilling Program, https://doi.org/10.2973/odp.proc.sr.201.109.2006, 2006.

Boudreau, B. P. and Westrich, J. T.: The dependence of bacterial sulfate reduction on sulfate concentration in marine sediments, Geochim. Cosmochim. Acta, 48, 2503–2516, https://doi.org/10.1016/0016-7037(84)90301-6, 1984.

Bradley, A. S., Leavitt, W. D., Schmidt, M., Knoll, A. H., Girguis, P. R., and Johnston, D. T.: Patterns of sulfur isotope fractionation during microbial sulfate reduction, Geobiology, 14, 91–101, 2016.

Brunner, B., Bernasconi, S. M., Kleikemper, J., and Schroth, M. H.: A model for oxygen and sulfur isotope fractionation in sulfate during bacterial sulfate reduction processes, Geochim. Cosmochim. Acta, 69, 4773–4785, https://doi.org/10.1016/j.gca.2005.04.017, 2005.

Campbell, K. A., Farmer, J. D., and Des Marais, D.: Ancient hydrocarbon seeps from the Mesozoic convergent margin of California: carbonate geochemistry, fluids and palaeoenvironments, Geofluids, 2, 63–94, https://doi.org/10.1046/j.1468-8123.2002.00022.x, 2002.

Chambers, L. A., Trudinger, P. A., Smith, J. W., and Burns, M. S.: Fractionation of sulfur isotopes by continuous cultures of Desulfovibrio desulfuricans, Can. J. Microbiol., 21, 1602–1607, 1975.

Chivian, D., Brodie, E. L., Alm, E. J., Culley, D. E., Dehal, P. S., DeSantis, T. Z., Gihring, T. M., Lapidus, A., Lin, L.-H., Lowry, S. R., Moser, D. P., Richardson, P. M., Southam, G., Wanger, G., Pratt, L. M., Andersen, G. L., Hazen, T. C., Brockman, F. J., Arkin, A. P., and Onstott, T. C.: Environmental Genomics Reveals a Single-Species Ecosystem Deep Within Earth, Science, 322, 275–278, https://doi.org/10.1126/science.1155495, 2008.

Coplen, T. B.: Discontinuance of SMOW and PDB, Nature, 375, 285, 1995.

Crameri, F., Shephard, G. E., and Heron, P. J.: The misuse of colour in science communication, Nat. Commun., 11, https://doi.org/10.1038/s41467-020-19160-7, 2020.

Crockford, P. W., Kunzmann, M., Bekker, A., Hayles, J., Bao, H., Halverson, G. P., Peng, Y., Bui, T. H., Cox, G. M., Gibson, T. M., Wörndle, S., Rainbird, R., Lepland, A., Swanson-Hysell, N. L., Master, S., Sreenivas, B., Kuznetsov, A., Krupenik, V., and Wing, B. A.: Claypool continued: Extending the isotopic record of sedimentary sulfate, Chem. Geol., 513, 200–225, https://doi.org/10.1016/j.chemgeo.2019.02.030, 2019.

Ding, T., Valkiers, S., Kipphardt, H., De Bièvre, P., Taylor, P. D. P., Gonfiantini, R., and Krouse, R.: Calibrated sulfur isotope abundance ratios of three IAEA sulfur isotope reference materials and V-CDT with a reassessment of the atomic weight of sulfur, Geochim. Cosmochim. Acta, 65, 2433–2437, https://doi.org/10.1016/S0016-7037(01)00611-1, 2001.

Drake, H. and Reiners, P. W.: Thermochronologic perspectives on the deep-time evolution of the deep biosphere, Proc. Natl. Acad. Sci. U.S.A., 118, e2109609118, https://doi.org/10.1073/pnas.2109609118, 2021.

Drake, H., Åström, M. E., Tullborg, E.-L., Whitehouse, M., and Fallick, A. E.: Variability of sulphur isotope ratios in pyrite and dissolved sulphate in granitoid fractures down to 1km depth – Evidence for widespread activity of sulphur reducing bacteria, Geochim. Cosmochim. Acta, 102, 143–161, https://doi.org/10.1016/j.gca.2012.10.036, 2013.

Drake, H., Åström, M. E., Heim, C., Broman, C., Åström, J., Whitehouse, M., Ivarsson, M., Siljeström, S., and Sjövall, P.: Extreme ^{13}C depletion of carbonates formed during oxidation of biogenic methane in fractured granite, Nat. Commun., 6, 7020, https://doi.org/10.1038/ncomms8020, 2015.

Drake, H., Heim, C., Roberts, N. M. W., Zack, T., Tillberg, M., Broman, C., Ivarsson, M., Whitehouse, M. J., and Åström, M. E.: Isotopic evidence for microbial production and consumption of methane in the upper continental crust throughout the Phanerozoic eon, Earth Planet. Sci. Lett., 470, 108–118, https://doi.org/10.1016/j.epsl.2017.04.034, 2017.

Drake, H., Whitehouse, M. J., Heim, C., Reiners, P. W., Tillberg, M., Hogmalm, K. J., Dopson, M., Broman, C., and Åström, M. E.: Unprecedented ^{34}S-enrichment of pyrite formed following microbial sulfate reduction in fractured crystalline rocks, Geobiology, 16, 556–574, https://doi.org/10.1111/gbi.12297, 2018.

Drake, H., Roberts, N. M. W., Reinhardt, M., Whitehouse, M., Ivarsson, M., Karlsson, A., Kooijman, E., and Kielman-Schmitt, M.: Biosignatures of ancient microbial life are present across the igneous crust of the Fennoscandian shield, Commun. Earth Environ., 2, 102, https://doi.org/10.1038/s43247-021-00170-2, 2021.

Drake, H., Makahnouk, W. R. M., Roberts, N. M. W., Reinhardt, M., Henkemans, E., Frape, S. K., Tullborg, L., Broman, C., Whitehouse, M. J., and Kooijman, E.: Late Cretaceous and Early Paleogene Fluid Circulation and Microbial Activity in Deep

Fracture Networks of the Precambrian Basement of Western Greenland, Geochem. Geophys. Geosyst., 25, e2024GC011646, 2024.

Farquhar, J., Johnston, D. T., Wing, B. A., Habicht, K. S., Canfield, D. E., Airieau, S., and Thiemens, M. H.: Multiple sulphur isotopic interpretations of biosynthetic pathways: implications for biological signatures in the sulphur isotope record, Geobiology, 1, 27–36, https://doi.org/10.1046/j.1472-4669.2003.00007.x, 2003.

Feng, D., Chen, D., Peckmann, J., and Bohrmann, G.: Authigenic carbonates from methane seeps of the northern Congo fan: Microbial formation mechanism, Mar. Pet. Geol., 27, 748–756, https://doi.org/10.1016/j.marpetgeo.2009.08.006, 2010.

Fichtner, V., Kirchner, F., Kutzschbach, M., Strauss, H., Tillberg, M., Whitehouse, M., and Drake, H.: Microscale $\delta^{34}S$ and $\delta^{18}O$ variations of barite as an archive for fluid mixing and microbial sulphur metabolisms in igneous rock aquifers, Isotopes Environ. Health Stud., 1–28, https://doi.org/10.1080/10256016.2024.2410293, 2024.

Fichtner, V., Genske, F., Kooijman, E., and Drake, H.: Carbonate-Associated Sulfate Does Not Record Superheavy $\delta^{34}S$ in Deep Scandinavian Bedrock Fractures: Implications for Pyrite Formation in the Deep Biosphere, Geochem. Geophys. Geosyst., 27, e2025GC012798, https://doi.org/10.1029/2025GC012798, 2026.

Fritz, P., Basharmal, G. M., Drimmie, R. J., Ibsen, J., and Qureshi, R. M.: Oxygen isotope exchange between sulphate and water during bacterial reduction of sulphate, Chem. Geol., 79, 99–105, https://doi.org/10.1016/0168-9622(89)90012-2, 1989.

Glossner, A. W., Gallagher, L. K., Landkamer, L., Figueroa, L., Munakata-Marr, J., and Mandernack, K. W.: Factors controlling the co-occurrence of microbial sulfate reduction and methanogenesis in coal bed reservoirs, Int. J. Coal Geol, 165, 121–132, https://doi.org/10.1016/j.coal.2016.08.012, 2016.

Göhring, A., Mauder, M., Kröger, P., and Grupe, G.: Using Gaussian Mixture Model clustering for multi-isotope analysis of archaeological fish bones for palaeobiodiversity studies, Rapid Comm. Mass Spectrom., 30, 1349–1360, https://doi.org/10.1002/rcm.7573, 2016.

Griffith, E. M. and Paytan, A.: Barite in the ocean – occurrence, geochemistry and palaeoceanographic applications, Sedimentology, 59, 1817–1835, https://doi.org/10.1111/j.1365-3091.2012.01327.x, 2012.

Gustafsson, J. and Drake, H.: Biosignatures of an ancient bedrock- and impact structure-hosted deep biosphere: current knowledge and future perspectives, Discov. Geosci., 3, 68, https://doi.org/10.1007/s44288-025-00176-9, 2025.

Habicht, K. S., Gade, M., Thamdrup, B., Berg, P., and Canfield, D. E.: Calibration of Sulfate Levels in the Archean Ocean, Science, 298, 2372–2374, 2002.

Halevy, I., Fike, D. A., Pasquier, V., Bryant, R. N., Wenk, C. B., Turchyn, A. V., Johnston, D. T., and Claypool, G. E.: Sedimentary parameters control the sulfur isotope composition of marine pyrite, Science, 382, 946–951, https://doi.org/10.1126/science.adh1215, 2023.

Hallbeck, L. and Pedersen, K.: Explorative analyses of microbes, colloids, and gases together with microbial modelling – Site description model SDM-Site Laxemar, R-08-109, Swedish Nuclear Fuel and Waste Management Co. (SKB), 2008.

Han, T., Bao, H., Peng, Y., Lu, Z., and Song, Y.: The barite record of the past seawater oxygen isotope composition, Nat. Commun., 16, 5018, https://doi.org/10.1038/s41467-025-60309-z, 2025.

Heinonen, A., Andersen, T., Rämö, O. T., and Whitehouse, M.: The source of Proterozoic anorthosite and rapakivi granite magmatism: evidence from combined in situ Hf–O isotopes of zircon in the Ahvenisto complex, southeastern Finland, J. Geol. Soc., 172, 103–112, https://doi.org/10.1144/jgs2014-013, 2015.

Herlambang, A., John, C. M., and Drake, H.: Physicochemical Conditions of the Devonian-Jurassic Continental Deep Biosphere Tracked by Carbonate Clumped Isotope Temperatures of Granite-Hosted Carbonate Veins, Geofluids, 2023, 1–10, https://doi.org/10.1155/2023/8445328, 2023.

Hoehler, T. M. and Jørgensen, B. B.: Microbial life under extreme energy limitation, Nat. Rev. Microbiol., 11, 83–94, https://doi.org/10.1038/nrmicro2939, 2013.

Ivarsson, M., Drake, H., Neubeck, A., Sallstedt, T., Bengtson, S., Roberts, N. M. W., and Rasmussen, B.: The fossil record of igneous rock, Earth-Sci. Rev., 210, 103342, https://doi.org/10.1016/j.earscirev.2020.103342, 2020.

Iversen, N. and Jorgensen, B. B.: Anaerobic methane oxidation rates at the sulfate-methane transition in marine sediments from Kattegat and Skagerrak (Denmark), Limnol. & Oceanogr., 30, 944–955, https://doi.org/10.4319/lo.1985.30.5.0944, 1985.

Jørgensen, B. B., Böttcher, M. E., Lüschen, H., Neretin, L. N., and Volkov, I. I.: Anaerobic methane oxidation and a deep H_2S sink generate isotopically heavy sulfides in Black Sea sediments, Geochim. Cosmochim. Acta, 68, 2095–2118, https://doi.org/10.1016/j.gca.2003.07.017, 2004.

Jørgensen, B. B., Findlay, A. J., and Pellerin, A.: The Biogeochemical Sulfur Cycle of Marine Sediments, Front. Microbiol., 10, 849, https://doi.org/10.3389/fmicb.2019.00849, 2019.

Kieft, T. L., Walters, C. C., Higgins, M. B., Mennito, A. S., Clewett, C. F. M., Heuer, V., Pullin, M. J., Hendrickson, S., Van Heerden, E., Sherwood Lollar, B., Lau, M. C. Y., and Onstott, T. C.: Dissolved organic matter compositions in 0.6–3.4 km deep fracture waters, Kaapvaal Craton, South Africa, Org. Geochem., 118, 116–131, https://doi.org/10.1016/j.orggeochem.2018.02.003, 2018.

Kotelnikova, S.: Microbial production and oxidation of methane in deep subsurface, Earth-Sci. Rev., 58, 367–395, https://doi.org/10.1016/S0012-8252(01)00082-4, 2002.

Küsel, K. and Dopson, M.: Groundwater microbial communities across the terrestrial subsurface, Nat. Microbiol., 11, 2088–2097, https://doi.org/10.1038/s41564-026-02427-y, 2026.

Laaksoharju, M., Smellie, J., Tullborg, E.-L., Gimeno, M., Hallbeck, L., Molinero, J., and Waber, N.: Bedrock hydrogeochemistry Forsmark- Site descriptive modelling - SDM-Site Forsmark, R-08-47, Swedish Nuclear Fuel and Waste Management Co. (SKB), Stockholm, Sweden, 2008.

Leavitt, W. D., Halevy, I., Bradley, A. S., and Johnston, D. T.: Influence of sulfate reduction rates on the Phanerozoic sulfur isotope record, Proc. Natl. Acad. Sci. U.S.A., 110, 11244–11249, https://doi.org/10.1073/pnas.1218874110, 2013.

Lin, Z., Wang, Q., Feng, D., Liu, Q., and Chen, D.: Post-depositional origin of highly ^{13}C-depleted carbonate in the Doushantuo cap dolostone in South China: Insights from petrography and stable carbon isotopes, Sediment. Geol., 242, 71–79, https://doi.org/10.1016/j.sedgeo.2011.10.009, 2011.

Liseroudi, M. H., Ardakani, O. H., Pedersen, P. K., Stern, R. A., Wood, J. M., and Sanei, H.: Microbial and thermochemical controlled sulfur cycle in the Early Triassic sediments of the Western Canadian Sedimentary Basin, J. Geol. Soc., 178, jgs2020-175, https://doi.org/10.1144/jgs2020-175, 2021.

Lyons, Wm. B. and Gaudette, H. E.: Sulfate reduction and the nature of organic matter in estuarine sediments, Org. Geochem., 1, 151–155, https://doi.org/10.1016/0146-6380(79)90003-2, 1979.

Machel, H. G.: Bacterial and thermochemical sulfate reduction in diagenetic settings – old and new insights, Sediment. Geol., 2001.

Magnabosco, C., Lin, L.-H., Dong, H., Bomberg, M., Ghiorse, W., Stan-Lotter, H., Pedersen, K., Kieft, T. L., Van Heerden, E., and Onstott, T. C.: The biomass and biodiversity of the continental subsurface, Nature Geosci, 11, 707–717, https://doi.org/10.1038/s41561-018-0221-6, 2018.

McMahon, S. and Parnell, J.: Weighing the deep continental biosphere, FEMS Microbiol. Ecol., 87, 113–120, https://doi.org/10.1111/1574-6941.12196, 2014.

McMahon, S. and Parnell, J.: The deep history of Earth's biomass, J. Geol. Soc., 175, 716–720, https://doi.org/10.1144/jgs2018-061, 2018.

Mizutani, Y. and Rafter, T. A.: Isotopic behaviour of sulphate oxygen in the bacterial reduction of sulphate, Geochem. J., 6, 183–191, 1973.

Natalicchio, M., Birgel, D., Dela Pierre, F., Martire, L., Clari, P., Spötl, C., and Peckmann, J.: Polyphasic carbonate precipitation in the shallow subsurface: Insights from microbially-formed authigenic carbonate beds in upper Miocene sediments of the Tertiary Piedmont Basin (NW Italy), Palaeogeogr. Palaeoclimatol. Palaeoecol., 329–330, 158–172, https://doi.org/10.1016/j.palaeo.2012.02.026, 2012.

Pallud, C. and Van Cappellen, P.: Kinetics of microbial sulfate reduction in estuarine sediments, Geochim. Cosmochim. Acta, 70, 1148–1162, https://doi.org/10.1016/j.gca.2005.11.002, 2006.

Pasquier, V., Marin-Carbonne, J., Giunta, T., Ruffine, L., and Halevy, I.: Microscale iron and sulphur isotopic compositions reveal pyritization pathways during early diagenesis, Commun. Earth Environ., 6, 248, https://doi.org/10.1038/s43247-025-02213-4, 2025.

Paytan, A., Kastner, M., Campbell, D., and Thiemens, M. H.: Sulfur Isotopic Composition of Cenozoic Seawater Sulfate, Science, 282, 1459–1462, https://doi.org/10.1126/science.282.5393.1459, 1998.

Paytan, A., Mearon, S., Cobb, K., and Kastner, M.: Origin of marine barite deposits: Sr and S isotope characterization, Geology, 30, 747, https://doi.org/10.1130/0091-7613(2002)030%3C0747:OOMBDS%3E2.0.CO;2, 2002.

Pedersen, K., Ekendahl, S., Tullborg, E.-L., Furnes, H., Thorseth, I., and Tumyr, O.: Evidence of ancient life at 207 m depth in a granitic aquifer, Geology, 25, 827–830, 1997.

Pedregosa, F., Varoquaux, G., Gramfort, A., Michel, V., Thirion, B., Grisel, O., Blondel, M., Prettenhofer, P., Weiss, R., Dubourg, V., Vanderplas, J., Passos, A., Brucher, M., Perrot, M., and Duchesnay, É.: Scikit-learn: Machine Learning in Python, J. Mach. Learn. Res., 12, 2825–2830, 2011.

Reitner, J., Peckmann, J., Reimer, A., Schumann, G., and Thiel, V.: Methane-derived carbonate build-ups and associated microbial communities at cold seeps on the lower Crimean shelf (Black Sea), Facies, 51, 66–79, https://doi.org/10.1007/s10347-005-0059-4, 2005.

Ries, J. B., Fike, D. A., Pratt, L. M., Lyons, T. W., and Grotzinger, J. P.: Superheavy pyrite ($\delta^{34}S_{pyr} > \delta^{34}S_{CAS}$) in the terminal Proterozoic Nama Group, southern Namibia: A consequence of low seawater sulfate at the dawn of animal life, Geology, 37, 743–746, https://doi.org/10.1130/G25775A.1, 2009.

Rubin-Blum, M., Antler, G., Turchyn, A. V., Tsadok, R., Goodman-Tchernov, B. N., Shemesh, E., Austin, J. A., Coleman, D. F., Makovsky, Y., Sivan, O., and Tchernov, D.: Hydrocarbon-related microbial processes in the deep sediments of the Eastern Mediterranean Levantine Basin, FEMS Microbiol. Ecol., 87, 780–796, https://doi.org/10.1111/1574-6941.12264, 2014.

Rudnicki, M. D., Elderfield, H., and Spiro, B.: Fractionation of sulfur isotopes during bacterial sulfate reduction in deep ocean sediments at elevated temperatures, Geochim. Cosmochim. Acta, 65, 777–789, https://doi.org/10.1016/S0016-7037(00)00579-2, 2001.

Ruff, S. E., De Angelis, I. H., Mullis, M., Payet, J. P., Magnabosco, C., Lloyd, K. G., Sheik, C. S., Steen, A. D., Shipunova, A., Morozov, A., Reese, B. K., Bradley, J. A., Lemonnier, C., Schrenk, M. O., Joye, S. B., Huber, J. A., Probst, A. J., Morrison, H. G., Sogin, M. L., Ladau, J., and Colwell, F.: A global comparison of surface and subsurface microbiomes reveals large-scale biodiversity gradients, and a marine-terrestrial divide, Sci. Adv., 10, eadq0645, https://doi.org/10.1126/sciadv.adq0645, 2024.

Runge, E. A., Mansor, M., Kappler, A., and Duda, J.-P.: Microbial biosignatures in ancient hydrothermal sulfides, Geobiology, 21, 355–377, 2023.

Schidlowski, M.: Carbon isotopes as biogeochemical recorders of life over 3.8 Ga of Earth history: evolution of a concept, Precambrian Res., 106, 117–134, https://doi.org/10.1016/S0301-9268(00)00128-5, 2001.

Sela-Adler, M., Ronen, Z., Herut, B., Antler, G., Vigderovich, H., Eckert, W., and Sivan, O.: Co-existence of Methanogenesis and Sulfate Reduction with Common Substrates in Sulfate-Rich Estuarine Sediments, Front. Microbiol., 8, 766, https://doi.org/10.3389/fmicb.2017.00766, 2017.

Sim, M. S., Bosak, T., and Ono, S.: Large Sulfur Isotope Fractionation Does Not Require Disproportionation, Science, 333, 74–77, https://doi.org/10.1126/science.1205103, 2011.

Stevens, T. O. and McKinley, J. P.: Lithoautotrophic Microbial Ecosystems in Deep Basalt Aquifers, Science, 270, 450–455, https://doi.org/10.1126/science.270.5235.450, 1995.

Strauss, H.: The isotopic composition of sedimentary sulfur through time, Palaeogeogr. Palaeoclim. Palaeoecol., 132, 97–118, 1997.

Takai, K., Nakamura, K., Toki, T., Tsunogai, U., Miyazaki, M., Miyazaki, J., Hirayama, H., Nakagawa, S., Nunoura, T., and Horikoshi, K.: Cell proliferation at 122°C and isotopically heavy CH4 production by a hyperthermophilic methanogen under high-pressure cultivation, Proc. Natl. Acad. Sci. U.S.A., 105, 10949–10954, https://doi.org/10.1073/pnas.0712334105, 2008.

Torres, M. E., Brumsack, H. J., Bohrmann, G., and Emeis, K. C.: Barite fronts in continental margin sediments: a new look at barium remobilization in the zone of sulfate reduction and formation of heavy barites in diagenetic fronts, Chem. Geol., 127, 125–139, https://doi.org/10.1016/0009-2541(95)00090-9, 1996.

Turchyn, A. V. and Schrag, D. P.: Oxygen Isotope Constraints on the Sulfur Cycle over the Past 10 Million Years, Science, 303, 2004–2007, https://doi.org/10.1126/science.1092296, 2004.

Turchyn, A. V. and Schrag, D. P.: Cenozoic evolution of the sulfur cycle: Insight from oxygen isotopes in marine sulfate, Earth Planet. Sci. Lett., 241, 763–779, https://doi.org/10.1016/j.epsl.2005.11.007, 2006.

Westrich, J. T. and Berner, R. A.: The role of sedimentary organic matter in bacterial sulfate reduction: The G model tested, Limnol. Oceanogr., 29, 236–249, https://doi.org/10.4319/lo.1984.29.2.0236, 1984.

Whitehouse, M. J.: Multiple Sulfur Isotope Determination by SIMS: Evaluation of Reference Sulfides for $\Delta^{33}S$ with Observations and a Case Study on the Determination of $\Delta^{36}S$, Geostand. Geoanal. Res., 37, 19–33, https://doi.org/10.1111/j.1751-908X.2012.00188.x, 2013.

Whiticar, M. J.: Carbon and hydrogen isotope systematics of bacterial formation and oxidation of methane, Chem. Geol., 161, 291–314, https://doi.org/10.1016/S0009-2541(99)00092-3, 1999.

Wing, B. A. and Halevy, I.: Intracellular metabolite levels shape sulfur isotope fractionation during microbial sulfate respiration, Proc. Natl. Acad. Sci. U.S.A., 111, 18116–18125, https://doi.org/10.1073/pnas.1407502111, 2014.

Wood, R. S., Lepland, A., Ogliore, R. C., Houghton, J., and Fike, D. A.: Microscale $\delta^{34}S$ heterogeneities in cold seep barite record variable methane flux off the Lofoten-Vesterålen Continental Margin, Norway, Earth Planet. Sci. Lett., 574, 117164, https://doi.org/10.1016/j.epsl.2021.117164, 2021.

Wortmann, U. G., Bernasconi, S. M., and Böttcher, M. E.: Hypersulfidic deep biosphere indicates extreme sulfur isotope fractionation during single-step microbial sulfate reduction, Geology, 29, 647, https://doi.org/10.1130/0091-7613(2001)029%3C0647:HDBIES%3E2.0.CO;2, 2001.

Wortmann, U. G., Chernyavsky, B., Bernasconi, S. M., Brunner, B., Böttcher, M. E., and Swart, P. K.: Oxygen isotope biogeochemistry of pore water sulfate in the deep biosphere: Dominance of isotope exchange reactions with ambient water during microbial sulfate reduction (ODP Site 1130), Geochim. Cosmochim. Acta, 71, 4221–4232, https://doi.org/10.1016/j.gca.2007.06.033, 2007.

Wu, X., Holmfeldt, K., Hubalek, V., Lundin, D., Åström, M., Bertilsson, S., and Dopson, M.: Microbial metagenomes from three aquifers in the Fennoscandian shield terrestrial deep biosphere reveal metabolic partitioning among populations, The ISME Journal, 10, 1192–1203, https://doi.org/10.1038/ismej.2015.185, 2016.

Yang, L. W., Yang, T., Li, J., Lin, Y., and Ling, H.-F.: The marine redox evolution and the formation model for the early Cambrian Gongxi-Tianzhu barite deposits in the South China Block, Ore Geol. Rev., 158, 105502, https://doi.org/10.1016/j.oregeorev.2023.105502, 2023.

York, D., Evensen, N. M., Martínez, M. L., and De Basabe Delgado, J.: Unified equations for the slope, intercept, and standard errors of the best straight line, Am. J. Phys., 72, 367–375, https://doi.org/10.1119/1.1632486, 2004.

Zaback, D. A., Pratt, L. M., and Hayes, J. M.: Transport and reduction of sulfate and immobilization of sulfide in marine black shales, Geology, 21, 141, https://doi.org/10.1130/0091-7613(1993)021%3C0141:TAROSA%3E2.3.CO;2, 1993.

Zan, B., Mou, C., Lash, G. G., Yan, J., and Hou, Q.: Diagenetic barite-calcite-pyrite nodules in the Silurian Longmaxi Formation of the Yangtze Block, South China: A plausible record of sulfate-methane transition zone movements in ancient marine sediments, Chem. Geol., 595, 120789, https://doi.org/10.1016/j.chemgeo.2022.120789, 2022.

Zhou, X., Chen, D., Dong, S., Zhang, Y., Guo, Z., Wei, H., and Yu, H.: Diagenetic barite deposits in the Yurtus Formation in Tarim Basin, NW China: Implications for barium and sulfur cycling in the earliest Cambrian, Precambrian Res., 263, 79–87, https://doi.org/10.1016/j.precamres.2015.03.006, 2015.

Seite 2: [1] hat gelöscht	**Runge, Eric**	**21.08.26 10:50:00**
Seite 2: [2] hat gelöscht	**Runge, Eric**	**21.08.26 10:50:00**
Seite 2: [3] hat gelöscht	**Runge, Eric**	**21.08.26 10:50:00**
Seite 2: [4] hat gelöscht	**Runge, Eric**	**21.08.26 10:50:00**
Seite 2: [5] hat gelöscht	**Runge, Eric**	**21.08.26 10:50:00**
Seite 3: [6] hat gelöscht	**Runge, Eric**	**21.08.26 10:50:00**
Seite 3: [7] hat gelöscht	**Runge, Eric**	**21.08.26 10:50:00**
Seite 3: [8] hat gelöscht	**Runge, Eric**	**21.08.26 10:50:00**
Seite 3: [9] hat gelöscht	**Runge, Eric**	**21.08.26 10:50:00**
Seite 7: [10] hat gelöscht	**Runge, Eric**	**21.08.26 10:50:00**
Seite 9: [11] hat gelöscht	**Runge, Eric**	**21.08.26 10:50:00**
Seite 9: [12] hat gelöscht	**Runge, Eric**	**21.08.26 10:50:00**
Seite 9: [13] hat gelöscht	**Runge, Eric**	**21.08.26 10:50:00**
Seite 9: [14] hat gelöscht	**Runge, Eric**	**21.08.26 10:50:00**
Seite 9: [15] hat gelöscht	**Runge, Eric**	**21.08.26 10:50:00**
Seite 9: [16] hat gelöscht	**Runge, Eric**	**21.08.26 10:50:00**

Seite 10: [17] hat gelöscht	**Runge, Eric**	**21.08.26 10:50:00**
Seite 10: [17] hat gelöscht	**Runge, Eric**	**21.08.26 10:50:00**
Seite 10: [17] hat gelöscht	**Runge, Eric**	**21.08.26 10:50:00**
Seite 10: [17] hat gelöscht	**Runge, Eric**	**21.08.26 10:50:00**
Seite 10: [18] hat gelöscht	**Runge, Eric**	**21.08.26 10:50:00**
Seite 10: [18] hat gelöscht	**Runge, Eric**	**21.08.26 10:50:00**
Seite 10: [19] hat gelöscht	**Runge, Eric**	**21.08.26 10:50:00**
Seite 10: [19] hat gelöscht	**Runge, Eric**	**21.08.26 10:50:00**
Seite 10: [19] hat gelöscht	**Runge, Eric**	**21.08.26 10:50:00**
Seite 10: [19] hat gelöscht	**Runge, Eric**	**21.08.26 10:50:00**
Seite 10: [19] hat gelöscht	**Runge, Eric**	**21.08.26 10:50:00**
Seite 10: [19] hat gelöscht	**Runge, Eric**	**21.08.26 10:50:00**
Seite 10: [19] hat gelöscht	**Runge, Eric**	**21.08.26 10:50:00**
Seite 10: [19] hat gelöscht	**Runge, Eric**	**21.08.26 10:50:00**
Seite 10: [19] hat gelöscht	**Runge, Eric**	**21.08.26 10:50:00**

Seite 10: [19] hat gelöscht	Runge, Eric	21.08.26 10:50:00
Seite 13: [20] hat gelöscht	Runge, Eric	21.08.26 10:50:00
Seite 14: [21] hat gelöscht	Runge, Eric	21.08.26 10:50:00
Seite 14: [22] hat gelöscht	Runge, Eric	21.08.26 10:50:00
Seite 14: [23] hat gelöscht	Runge, Eric	21.08.26 10:50:00
Seite 14: [24] hat gelöscht	Runge, Eric	21.08.26 10:50:00
Seite 14: [25] hat gelöscht	Runge, Eric	21.08.26 10:50:00
Seite 14: [26] hat gelöscht	Runge, Eric	21.08.26 10:50:00
Seite 14: [27] hat gelöscht	Runge, Eric	21.08.26 10:50:00
Seite 15: [28] hat gelöscht	Runge, Eric	21.08.26 10:50:00
Seite 15: [28] hat gelöscht	Runge, Eric	21.08.26 10:50:00
Seite 15: [28] hat gelöscht	Runge, Eric	21.08.26 10:50:00
Seite 15: [28] hat gelöscht	Runge, Eric	21.08.26 10:50:00
Seite 15: [28] hat gelöscht	Runge, Eric	21.08.26 10:50:00
Seite 15: [28] hat gelöscht	Runge, Eric	21.08.26 10:50:00
Seite 17: [29] hat gelöscht	Runge, Eric	21.08.26 10:50:00
Seite 17: [29] hat gelöscht	Runge, Eric	21.08.26 10:50:00

Seite 17: [29] hat gelöscht	**Runge, Eric**	**21.08.26 10:50:00**
Seite 17: [29] hat gelöscht	**Runge, Eric**	**21.08.26 10:50:00**
Seite 17: [29] hat gelöscht	**Runge, Eric**	**21.08.26 10:50:00**
Seite 17: [29] hat gelöscht	**Runge, Eric**	**21.08.26 10:50:00**
Seite 17: [29] hat gelöscht	**Runge, Eric**	**21.08.26 10:50:00**
Seite 17: [30] hat gelöscht	**Runge, Eric**	**21.08.26 10:50:00**
Seite 17: [31] hat gelöscht	**Runge, Eric**	**21.08.26 10:50:00**
Seite 17: [32] hat gelöscht	**Runge, Eric**	**21.08.26 10:50:00**
Seite 17: [33] hat gelöscht	**Runge, Eric**	**21.08.26 10:50:00**
Seite 17: [33] hat gelöscht	**Runge, Eric**	**21.08.26 10:50:00**
Seite 17: [33] hat gelöscht	**Runge, Eric**	**21.08.26 10:50:00**
Seite 17: [33] hat gelöscht	**Runge, Eric**	**21.08.26 10:50:00**
Seite 17: [33] hat gelöscht	**Runge, Eric**	**21.08.26 10:50:00**

Seite 17: [33] hat gelöscht	**Runge, Eric**	**21.08.26 10:50:00**
Seite 17: [33] hat gelöscht	**Runge, Eric**	**21.08.26 10:50:00**
Seite 17: [33] hat gelöscht	**Runge, Eric**	**21.08.26 10:50:00**
Seite 17: [33] hat gelöscht	**Runge, Eric**	**21.08.26 10:50:00**
Seite 17: [33] hat gelöscht	**Runge, Eric**	**21.08.26 10:50:00**
Seite 17: [33] hat gelöscht	**Runge, Eric**	**21.08.26 10:50:00**
Seite 17: [33] hat gelöscht	**Runge, Eric**	**21.08.26 10:50:00**
Seite 17: [33] hat gelöscht	**Runge, Eric**	**21.08.26 10:50:00**
Seite 17: [33] hat gelöscht	**Runge, Eric**	**21.08.26 10:50:00**
Seite 17: [33] hat gelöscht	**Runge, Eric**	**21.08.26 10:50:00**
Seite 17: [33] hat gelöscht	**Runge, Eric**	**21.08.26 10:50:00**
Seite 17: [33] hat gelöscht	**Runge, Eric**	**21.08.26 10:50:00**
Seite 17: [33] hat gelöscht	**Runge, Eric**	**21.08.26 10:50:00**
Seite 17: [33] hat gelöscht	**Runge, Eric**	**21.08.26 10:50:00**
Seite 17: [33] hat gelöscht	**Runge, Eric**	**21.08.26 10:50:00**
Seite 17: [33] hat gelöscht	**Runge, Eric**	**21.08.26 10:50:00**

Seite 17: [33] hat gelöscht	**Runge, Eric**	**21.08.26 10:50:00**

Seite 17: [33] hat gelöscht	**Runge, Eric**	**21.08.26 10:50:00**